[3] P.L. Dahia, R.C. Aguiar, J. Alberta, J.B. Kum, S. Caron, H. Sill, D.J. Marsh, J. Ritz, A. Freedman, C. Stiles, C. Eng, PTEN is inversely correlated with the cell survival factor Akt/PKB and is inactivated via multiple mechanisms in haematological malignancies, Hum. Mol. Genet. 8 (1999) 185–193.
[4] G.C. Fillmore, Q. Wang, M.J. Carey, C.H. Kim, K.S. Elenitoba-Johnson, M.S. Lim, Expression of Akt (protein kinase B) and its isoforms in malignant lymphomas, Leuk. Lymphoma 46 (2005) 1765–1773.
[5] W.H. Shen, A.S. Balajee, J. Wang, H. Wu, C. Eng, P.P. Pandolfi, Y. Yin, Essential role for nuclear PTEN in maintaining chromosomal integrity, Cell 128 (2007) 157–170.
[6] I.U. Ali, L.M. Schriml, M. Dean, Mutational spectra of PTEN/MMAC1 gene: a tumor suppressor with lipid phosphatase activity, J. Natl. Cancer Inst. 91 (1999) 1922–1932.
[7] D. Bonneau, M. Longy, Mutations of the human PTEN gene, Hum. Mutat. 16 (2000) 109–122.
[8] Y. Yin, W.H. Shen, PTEN: a new guardian of the genome, Oncogene 27 (2008) 5443–5453.
[9] L.C. Cantley, B.G. Neel, New insights into tumor suppression: PTEN suppresses tumor formation by restraining the phosphoinositide 3-kinase/AKT pathway, Proc. Natl. Acad. Sci. U.S.A. 96 (1999) 4240–4245.
[10] D. Liaw, D.J. Marsh, J. Li, P.L. Dahia, S.I. Wang, Z. Zheng, S. Bose, K.M. Call, H.C. Tsou, M. Peacocke, C. Eng, R. Parsons, Germline mutations of the PTEN gene in Cowden disease, an inherited breast and thyroid cancer syndrome, Nat. Genet. 16 (1997) 64–67.
[11] J.M. Garcia, J. Silva, C. Pena, V. Garcia, R. Rodriguez, M.A. Cruz, B. Cantos, M. Provencio, P. Espana, F. Bonilla, Promoter methylation of the PTEN gene is a common molecular change in breast cancer, Genes Chromosomes Cancer 41 (2004) 117–124.
[12] Y.H. Kang, H.S. Lee, W.H. Kim, Promoter methylation and silencing of PTEN in gastric carcinoma, Lab. Invest. 82 (2002) 285–291.
[13] F. Meng, R. Henson, H. Wehbe-Janek, K. Ghoshal, S.T. Jacob, T. Patel, MicroRNA-21 regulates expression of the PTEN tumor suppressor gene in human hepatocellular cancer, Gastroenterology 133 (2007) 647–658.
[14] H. Yang, W. Kong, L. He, J.J. Zhao, J.D. O'Donnell, J. Wang, R.M. Wenham, D. Coppola, P.A. Kruk, S.V. Nicosia, J.Q. Cheng, MicroRNA expression profiling in human ovarian cancer: miR-214 induces cell survival and cisplatin resistance by targeting PTEN, Cancer Res. 68 (2008) 425–433.
[15] K. Sircar, M. Yoshimoto, F.A. Monzon, I.H. Koumakpayi, R.L. Katz, A. Khanna, K. Alvarez, G. Chen, A.D. Darnel, A.G. Aprikian, F. Saad, T.A. Bismar, J.A. Squire, PTEN genomic deletion is associated with p-Akt and AR signalling in poorer outcome, hormone refractory prostate cancer, J. Pathol. 218 (2009) 505–513.
[16] Y. Shang, S. Kakinuma, Y. Amasaki, M. Nishimura, Y. Kobayashi, Y. Shimada, Aberrant activation of interleukin-9 receptor and downstream Stat3/5 in primary T-cell lymphomas in vivo in susceptible B6 and resistant C3H mice, In Vivo 22 (2008) 713–720.
[17] M. Malumbres, I. Perez de Castro, J. Santos, B. Melendez, R. Mangues, M. Serrano, A. Pellicer, J. Fernandez-Piqueras, Inactivation of the cyclin-dependent kinase inhibitor p15INK4b by deletion and de novo methylation with independence of p16INK4a alterations in murine primary T-cell lymphomas, Oncogene 14 (1997) 1361–1370.
[18] S. Kakinuma, M. Nishimura, S. Sasanuma, K. Mita, G. Suzuki, Y. Katsura, T. Sado, Y. Shimada, Spectrum of Znfn1a1 (Ikaros) inactivation and its association with loss of heterozygosity in radiogenic T-cell lymphomas in susceptible B6C3F1 mice, Radiat. Res. 157 (2002) 331–340.
[19] H. Okano, Y. Saito, T. Miyazawa, T. Shinbo, D. Chou, S. Kosugi, Y. Takahashi, S. Odani, O. Niwa, R. Kominami, Homozygous deletions and point mutations of the Ikaros gene in gamma-ray-induced mouse thymic lymphomas, Oncogene 18 (1999) 6677–6683.
[20] H. Tsuji, H. Ishii-Ohba, H. Ukai, T. Katsube, T. Ogiu, Radiation-induced deletions in the 5′ end region of Notch1 lead to the formation of truncated proteins and are involved in the development of mouse thymic lymphomas, Carcinogenesis 24 (2003) 1257–1268.
[21] D.P. Hong, K. Kubo, N. Tsugawa, N. Mori, S. Umesako, C.W. Song, M. Okumoto, Generation of large homozygous chromosomal segments by mitotic recombination during lymphomagenesis in F1 hybrid mice, J. Radiat. Res. (Tokyo) 43 (2002) 187–194.
[22] J. Santos, M. Herranz, M. Fernandez, C. Vaquero, P. Lopez, J. Fernandez-Piqueras, Evidence of a possible epigenetic inactivation mechanism operating on a region of mouse chromosome 19 in gamma-radiation-induced thymic lymphomas, Oncogene 20 (2001) 2186–2189.
[23] Y. Shimada, M. Nishimura, S. Kakinuma, M. Okumoto, T. Shiroishi, K.H. Clifton, S. Wakana, Radiation-associated loss of heterozygosity at the Znfn1a1 (Ikaros) locus on chromosome 11 in murine thymic lymphomas, Radiat. Res. 154 (2000) 293–300.
[24] P. Chomczynski, N. Sacchi, Single-step method of RNA isolation by acid guanidinium thiocyanate–phenol-chloroform extraction, Anal. Biochem. 162 (1987) 156–159.
[25] H. Ohi, Y. Mishima, K. Kamimura, M. Maruyama, K. Sasai, R. Kominami, Multistep lymphomagenesis deduced from DNA changes in thymic lymphomas and atrophic thymuses at various times after gamma-irradiation, Oncogene 26 (2007) 5280–5289.
[26] J. Roman-Gomez, A. Jimenez-Velasco, X. Agirre, F. Prosper, A. Heiniger, A. Torres, Lack of CpG island methylator phenotype defines a clinical subtype of T-cell acute lymphoblastic leukemia associated with good prognosis, J. Clin. Oncol. 23 (2005) 7043–7049.
[27] J.C. Soria, H.Y. Lee, J.I. Lee, L. Wang, J.P. Issa, B.L. Kemp, D.D. Liu, J.M. Kurie, L. Mao, F.R. Khuri, Lack of PTEN expression in non-small cell lung cancer could be related to promoter methylation, Clin. Cancer Res. 8 (2002) 1178–1184.
[28] J.M. Luo, Z.L. Liu, H.L. Hao, F.X. Wang, Z.R. Dong, R. Ohno, Mutation analysis of SHIP gene in acute leukemia, Zhongguo Shi Yan Xue Ye Xue Za Zhi 12 (2004) 420–426.
[29] A. Gutierrez, T. Sanda, R. Grebliunaite, A. Carracedo, L. Salmena, Y. Ahn, S. Dahlberg, D. Neuberg, L.A. Moreau, S.S. Winter, R. Larson, J. Zhang, A. Protopopov, L. Chin, P.P. Pandolfi, L.B. Silverman, S.P. Hunger, S.E. Sallan, A.T. Look, High frequency of PTEN, PI3K and AKT abnormalities in T cell acute lymphoblastic leukemia, Blood (2009).
[30] G.L. Huang, X.H. Zhang, G.L. Guo, K.T. Huang, K.Y. Yang, X.Q. Hu, Expression of microRNA-21 in invasive ductal carcinoma of the breast and its association with phosphatase and tensin homolog deleted from chromosome expression and clinicopathologic features, Zhonghua Yi Xue Za Zhi 88 (2008) 2833–2837.
[31] J.T. Huse, C. Brennan, D. Hambardzumyan, B. Wee, J. Pena, S.H. Rouhanifard, C. Sohn-Lee, C. le Sage, R. Agami, T. Tuschl, E.C. Holland, The PTEN-regulating microRNA miR-26a is amplified in high-grade glioma and facilitates gliomagenesis in vivo, Genes Dev. 23 (2009) 1327–1337.
[32] M.G. Pezzolesi, P. Platzer, K.A. Waite, C. Eng, Differential expression of PTEN-targeting microRNAs miR-19a and miR-21 in Cowden syndrome, Am. J. Hum. Genet. 82 (2008) 1141–1149.
[33] S. Roy, S. Khanna, S.R. Hussain, S. Biswas, A. Azad, C. Rink, S. Gnyawali, S. Shilo, G.J. Nuovo, C.K. Sen, MicroRNA expression in response to murine myocardial infarction: miR-21 regulates fibroblast metalloprotease-2 via phosphatase and tensin homologue, Cardiovasc. Res. 82 (2009) 21–29.
[34] H. Chang, X.Y. Qi, J. Claudio, L. Zhuang, B. Patterson, A.K. Stewart, Analysis of PTEN deletions and mutations in multiple myeloma, Leuk. Res. 30 (2006) 262–265.
[35] J.J. Scarisbrick, A.J. Woolford, R. Russell-Jones, S.J. Whittaker, Loss of heterozygosity on 10q and microsatellite instability in advanced stages of primary cutaneous T-cell lymphoma and possible association with homozygous deletion of PTEN, Blood 95 (2000) 2937–2942.
[36] A. Aggerholm, K. Gronbaek, P. Guldberg, P. Hokland, Mutational analysis of the tumour suppressor gene MMAC1/PTEN in malignant myeloid disorders, Eur. J. Haematol. 65 (2000) 109–113.
[37] K. Gronbaek, J. Zeuthen, P. Guldberg, E. Ralfkiaer, K. Hou-Jensen, Alterations of the MMAC1/PTEN gene in lymphoid malignancies, Blood 91 (1998) 4388–4390.
[38] G. Lenz, G.W. Wright, N.C. Emre, H. Kohlhammer, S.S. Dave, R.E. Davis, S. Carty, L.T. Lam, A.L. Shaffer, W. Xiao, J. Powell, A. Rosenwald, G. Ott, H.K. Muller-Hermelink, R.D. Gascoyne, J.M. Connors, E. Campo, E.S. Jaffe, J. Delabie, E.B. Smeland, L.M. Rimsza, R.I. Fisher, D.D. Weisenburger, W.C. Chan, L.M. Staudt, Molecular subtypes of diffuse large B-cell lymphoma arise by distinct genetic pathways, Proc. Natl. Acad. Sci. U.S.A. 105 (2008) 13520–13525.
[39] R.S. Maser, B. Choudhury, P.J. Campbell, B. Feng, K.K. Wong, A. Protopopov, J. O'Neil, A. Gutierrez, E. Ivanova, I. Perna, E. Lin, V. Mani, S. Jiang, K. McNamara, S. Zaghlul, S. Edkins, C. Stevens, C. Brennan, E.S. Martin, R. Wiedemeyer, O. Kabbarah, C. Nogueira, G. Histen, J. Aster, M. Mansour, V. Duke, L. Foroni, A.K. Fielding, A.H. Goldstone, J.M. Rowe, Y.A. Wang, A.T. Look, M.R. Stratton, L. Chin, P.A. Futreal, R.A. DePinho, Chromosomally unstable mouse tumours have genomic alterations similar to diverse human cancers, Nature 447 (2007) 966–971.
[40] Y. Nakahara, H. Nagai, T. Kinoshita, T. Uchida, S. Hatano, T. Murate, H. Saito, Mutational analysis of the PTEN/MMAC1 gene in non-Hodgkin's lymphoma, Leukemia 12 (1998) 1277–1280.
[41] T. Palomero, M.L. Sulis, M. Cortina, P.J. Real, K. Barnes, M. Ciofani, E. Caparros, J. Buteau, K. Brown, S.L. Perkins, G. Bhagat, A.M. Agarwal, G. Basso, M. Castillo, S. Nagase, C. Cordon-Cardo, R. Parsons, J.C. Zuniga-Pflucker, M. Dominguez, A.A. Ferrando, Mutational loss of PTEN induces resistance to NOTCH1 inhibition in T-cell leukemia, Nat. Med. 13 (2007) 1203–1210.
[42] A. Sakai, C. Thieblemont, A. Wellmann, E.S. Jaffe, M. Raffeld, PTEN gene alterations in lymphoid neoplasms, Blood 92 (1998) 3410–3415.
[43] R. Opavsky, S.H. Wang, P. Trikha, A. Raval, Y. Huang, Y.Z. Wu, B. Rodriguez, B. Keller, S. Liyanarachchi, G. Wei, R.V. Davuluri, M. Weinstein, D. Felsher, M. Ostrowski, G. Leone, C. Plass, CpG island methylation in a mouse model of lymphoma is driven by the genetic configuration of tumor cells, PLoS Genet. 3 (2007) 1757–1769.
[44] Y. Shimada, M. Nishimura, S. Kakinuma, T. Ogiu, H. Fujimoto, A. Kubo, J. Nagai, K. Kobayash, K. Tano, S. Yoshinaga, K.K. Bhakat, Genetic susceptibility to thymic lymphomas and K-ras gene mutation in mice after exposure to X-rays and N-ethyl-N-nitrosourea, Int. J. Radiat. Biol. 79 (2003) 423–430.
[45] T. Takabatake, S. Kakinuma, T. Hirouchi, M.M. Nakamura, K. Fujikawa, M. Nishimura, Y. Oghiso, Y. Shimada, K. Tanaka, Analysis of changes in DNA copy number in radiation-induced thymic lymphomas of susceptible C57BL/6, resistant C3H and hybrid F1 Mice, Radiat. Res. 169 (2008) 426–436.
[46] M. Yoshimoto, I.W. Cunha, R.A. Coudry, F.P. Fonseca, C.H. Torres, F.A. Soares, J.A. Squire, FISH analysis of 107 prostate cancers shows that PTEN genomic deletion is associated with poor clinical outcome, Br. J. Cancer 97 (2007) 678–685.
[47] N. Kawamata, S. Ogawa, M. Zimmermann, M. Kato, M. Sanada, K. Hemminki, G. Yamatomo, Y. Nannya, R. Koehler, T. Flohr, C.W. Miller, J. Harbott, W.D. Ludwig, M. Stanulla, M. Schrappe, C.R. Bartram, H.P. Koeffler, Molecular allelokaryotyping of pediatric acute lymphoblastic leukemias by high-resolution single nucleotide polymorphism oligonucleotide genomic microarray, Blood 111 (2008) 776–784.

[48] C.G. Mullighan, S. Goorha, I. Radtke, C.B. Miller, E. Coustan-Smith, J.D. Dalton, K. Girtman, S. Mathew, J. Ma, S.B. Pounds, X. Su, C.H. Pui, M.V. Relling, W.E. Evans, S.A. Shurtleff, J.R. Downing, Genome-wide analysis of genetic alterations in acute lymphoblastic leukaemia, Nature 446 (2007) 758–764.
[49] C.G. Mullighan, C.B. Miller, I. Radtke, L.A. Phillips, J. Dalton, J. Ma, D. White, T.P. Hughes, M.M. Le Beau, C.H. Pui, M.V. Relling, S.A. Shurtleff, J.R. Downing, BCR-ABL1 lymphoblastic leukaemia is characterized by the deletion of Ikaros, Nature 453 (2008) 110–114.
[50] K. Paulsson, J.B. Cazier, F. Macdougall, J. Stevens, I. Stasevich, N. Vrcelj, T. Chaplin, D.M. Lillington, T.A. Lister, B.D. Young, Microdeletions are a general feature of adult and adolescent acute lymphoblastic leukemia: unexpected similarities with pediatric disease, Proc. Natl. Acad. Sci. U.S.A. 105 (2008) 6708–6713.
[51] A. Usvasalo, S. Savola, R. Raty, K. Vettenranta, A. Harila-Saari, P. Koistinen, E.R. Savolainen, E. Elonen, U.M. Saarinen-Pihkala, S. Knuutila, CDKN2A deletions in acute lymphoblastic leukemia of adolescents and young adults: an array CGH study, Leuk. Res. 32 (2008) 1228–1235.
[52] J. Sakata, J. Inoue, H. Ohi, H. Kosugi-Okano, Y. Mishima, K. Hatakeyama, O. Niwa, R. Kominami, Involvement of V(D)J recombinase in the generation of intragenic deletions in the Rit1/Bcl11b tumor suppressor gene in gamma-ray-induced thymic lymphomas and in normal thymus of the mouse, Carcinogenesis 25 (2004) 1069–1075.
[53] H. Tsuji, H. Ishii-Ohba, T. Katsube, H. Ukai, S. Aizawa, M. Doi, K. Hioki, T. Ogiu, Involvement of illegitimate V(D)J recombination or microhomology-mediated nonhomologous end-joining in the formation of intragenic deletions of the Notch1 gene in mouse thymic lymphomas, Cancer Res. 64 (2004) 8882–8890.
[54] F. Novara, S. Beri, M.E. Bernardo, R. Bellazzi, A. Malovini, R. Ciccone, A.M. Cometa, F. Locatelli, R. Giorda, O. Zuffardi, Different molecular mechanisms causing 9p21 deletions in acute lymphoblastic leukemia of childhood, Hum. Genet. (2009).
[55] L.H. Saal, S.K. Gruvberger-Saal, C. Persson, K. Lovgren, M. Jumppanen, J. Staaf, G. Jonsson, M.M. Pires, M. Maurer, K. Holm, S. Koujak, S. Subramaniyam, J. Vallon-Christersson, H. Olsson, T. Su, L. Memeo, T. Ludwig, S.P. Ethier, M. Krogh, M. Szabolcs, V.V. Murty, J. Isola, H. Hibshoosh, R. Parsons, A. Borg, Recurrent gross mutations of the PTEN tumor suppressor gene in breast cancers with deficient DSB repair, Nat. Genet. 40 (2008) 102–107.
[56] P.O. Frappart, Y. Lee, H.R. Russell, N. Chalhoub, Y.D. Wang, K.E. Orii, J. Zhao, N. Kondo, S.J. Baker, P.J. McKinnon, Recurrent genomic alterations characterize medulloblastoma arising from DNA double-strand break repair deficiency, Proc. Natl. Acad. Sci. U.S.A. 106 (2009) 1880–1885.
[57] R.L. Pinsonneault, P.M. Vacek, J.P. O'Neill, B.A. Finette, Induction of V(D)J-mediated recombination of an extrachromosomal substrate following exposure to DNA-damaging agents, Environ. Mol. Mutagen. 48 (2007) 440–450.
[58] A.G. Knudson Jr., Mutation and cancer: statistical study of retinoblastoma, Proc. Natl. Acad. Sci. U.S.A. 68 (1971) 820–823.
[59] A. Di Cristofano, M. De Acetis, A. Koff, C. Cordon-Cardo, P.P. Pandolfi, Pten and p27KIP1 cooperate in prostate cancer tumor suppression in the mouse, Nat. Genet. 27 (2001) 222–224.
[60] L.C. Trotman, M. Niki, Z.A. Dotan, J.A. Koutcher, A. Di Cristofano, A. Xiao, A.S. Khoo, P. Roy-Burman, N.M. Greenberg, T. Van Dyke, C. Cordon-Cardo, P.P. Pandolfi, Pten dose dictates cancer progression in the prostate, PLoS Biol. 1 (2003) E59.
[61] J.H. Mao, D. Wu, J. Perez-Losada, H. Nagase, R. DelRosario, A. Balmain, Genetic interactions between Pten and p53 in radiation-induced lymphoma development, Oncogene 22 (2003) 8379–8385.
[62] M. Santarosa, A. Ashworth, Haploinsufficiency for tumour suppressor genes: when you don't need to go all the way, Biochim. Biophys. Acta 1654 (2004) 105–122.

RADIATION RESEARCH 173, 310–318 (2010)
0033-7587/10 $15.00
© 2010 by Radiation Research Society.
All rights of reproduction in any form reserved.
DOI: 10.1667/RR1905.1

Unique Characteristics of Radiation-Induced Apoptosis in the Postnatally Developing Small Intestine and Colon of Mice

T. Miyoshi-Imamura,[a,b] S. Kakinuma,[b] M. Kaminishi,[b] M. Okamoto,[b] T. Takabatake,[b] Y. Nishimura,[b] T. Imaoka,[b] M. Nishimura,[b] K. Murakami-Murofushi[a] and Y. Shimada[b,1]

[a] *Genetic Counseling Program, Graduate School of Humanities and Sciences, Ochanomizu University, 2-1-1 Otsuka, Bunkyo-ku, Tokyo, 112-8610, Japan; and* [b] *Experimental Radiology for Children's Health Research Group, National Institute of Radiological Sciences, 4-9-1 Anagawa, Inage-ku, Chiba, 263-8555, Japan*

Miyoshi-Imamura, T., Kakinuma, S., Kaminishi, M., Okamoto, M., Takabatake, T., Nishimura, Y., Imaoka, T., Nishimura, M., Murakami-Murofushi, K. and Shimada, Y. Unique Characteristics of Radiation-Induced Apoptosis in the Postnatally Developing Small Intestine and Colon of Mice. *Radiat. Res.* 173, 310–318 (2010).

We examined the response of the developing mouse intestine to X radiation using neonates (1 day postpartum), infants (2 weeks postpartum) and adults (7 weeks postpartum). Irradiated adult small intestinal crypts displayed two waves of apoptosis. The first wave peaked at 3 h and was followed by a broad wave with a peak persisting from 24 to 48 h. p53 was expressed during the first wave but not the second wave. For the infant small intestine, the intensity of the first wave was approximately half that of the adult wave, and for the colon the intensity was even smaller. In neonates, apoptosis was delayed, peaking at 6 h for small intestinal crypts and at 24 h for colonic crypts. Although no apoptosis occurred at 3 h postirradiation in neonates, p53 was present in both the small intestine and colon, owing at least in part to the inability of p53 to increase the level of Noxa, a p53-dependent pro-apoptosis protein, suggesting a discontinuity in the p53-Noxa-caspase pathway in neonates. By contrast, the induction of p21, a pro-survival protein, was greater in neonatal cells than in adult cells. Thus it appears that the developing and adult intestine mount distinct apoptotic responses to radiation. © 2010 by Radiation Research Society

INTRODUCTION

Fetuses and young children should not be considered simply as small adults but rather as a unique cohort when assessing the health risks of exposure to environmental carcinogens such as ionizing radiation. Members of this cohort appear to be especially vulnerable to radiation because their organs grow more rapidly and are less differentiated than those of adults. Radiation damage to the tissues has been shown to depend on the degree of cell proliferation and the extent of differentiation. A century ago, Bergonie and Tribondeau stated that "tissues appear to be more radiosensitive if their cells have a greater proliferative capacity, divide more rapidly, and are less-well differentiated" (*1*). The cells of the developing cerebral cortex and the developing kidney are highly susceptible to radiation-induced apoptosis—a sensitivity that is lost after differentiation (*2, 3*). Irradiated hematopoietic and mammary stem cells of weanling mice have been shown to be more severely damaged than those of adult mice (*4, 5*). Exposure of infant mice to 1.5 Gy of radiation depresses their levels of hematopoietic stem cells for a long time thereafter (*6*).

Apoptosis is a form of programmed cell death, i.e., a genetically controlled self-destruction process, occurring during developmental tissue morphogenesis and adult tissue homeostasis (*7*). Apoptosis can be induced by exposure to exogenous DNA-damaging agents including ionizing radiation. Intestinal tract organs of wild-type and genetically engineered adult mice have been used extensively as *in vivo* systems to assess the effects of radiation-induced apoptosis (*8*). The properties that have been monitored include dose response, temporal patterns of apoptosis, spatial distribution of susceptible cells in crypts, differential susceptibilities of small intestinal and colonic epithelial cells and of regions within the colon, and p53, p21 and Bcl-2 activities (*9–24*). However, similar studies using the intestines of neonates and infants have not been undertaken. Therefore, in this study we characterized the features of radiation-induced apoptosis in the postnatally developing small intestine and colon of C57BL/6J mice and compared these features to those of identically treated adult mice. We found that the postnatally developing intestine is more resistant to radiation-induced apoptosis than with the adult intestine, which could be ascribed in part to an apparent inability to completely carry out the post-p53-mediated pathway to apoptosis.

[1] Address for correspondence: Experimental Radiology for Children's Health Research Group, National Institute of Radiological Sciences, 4-9-1 Anagawa, Inage-ku, Chiba, 263-8555, Japan; e-mail: y_shimad@nirs.go.jp.

MATERIALS AND METHODS

Mice

Female C57BL/6J mice were purchased from Charles River Laboratories (Kanagawa, Japan). All mice were exposed to a 12-h dark-light cycle, a temperature of 23 ± 2°C, and 50 ± 10% humidity. They were fed a standard laboratory diet (MB-1; Funabashi Farm Co., Ltd., Chiba, Japan) and given water *ad libitum*. The experimental protocol was reviewed and approved by our institution's animal use committee.

Irradiation of Mice

Irradiation was performed using a Pantak X-ray generator (Pantak Ltd., East Haven, CT). One-day-old (neonate), 2-week-old (infant), and 7-week-old (adult) mice were whole-body irradiated with 2 Gy at a dose rate of 0.7 Gy/min (200 kVp, 20 mA, with a filter composed of 0.5-mm-thick copper and aluminum plates). Subsequently, mice were killed humanely at 0 (unirradiated), 3, 6, 12, 24, 48 and 72 h after irradiation.

Pathology

Unirradiated and irradiated mice were killed after ether anesthesia. Then their small intestines and colons were removed, rinsed in ice-cold phosphate-buffered saline, and fixed quickly in 10% neutral-buffered formalin for about 12 h. Each organ was divided into proximal, middle and distal sections. All samples were embedded in paraffin, sectioned transversely (3–4 μm thick), and stained with hematoxylin and eosin.

Immunohistochemistry

Immunostaining of paraffin-embedded samples followed standard procedures. To retrieve antigens using the primary antibodies [rabbit polyclonal anti-active caspase-3 (1:750, AF835; R&D Systems, Abingdon, UK); rabbit polyclonal anti-p53 (1:500, NCL-p53-CM5; Novocastral Laboratories Ltd., Newcastle, UK); rabbit polyclonal anti-Noxa (1:100, LS-B184/6830; LifeSpan Biosciences, Seattle, WA); rabbit polyclonal anti-p21 (1:500, sc397; Santa Cruz Biotechnology Inc., Santa Cruz, CA); and rat polyclonal anti-Ki-67 (1:100, M7249; DAKO Carpinteria, CA)], the tissue sections in 10 m*M* sodium citrate, pH 6.0, were heated at 120°C for 20 min. After the primary antibodies were washed away, sections were incubated with a peroxidase-conjugated secondary antibody [Histofine® Simple Stain MAX PO(R) or Histofine® Simple Stain MAX PO(Rat); Nichirei Biosciences, Tokyo, Japan]. Peroxidase activity was visualized by first staining with 3,3′-diaminobenzidine (Simple Stain DAB Solution, Nichirei Biosciences, Tokyo, Japan) and then counterstaining with hematoxylin.

Scoring the Numbers and Types of Small Intestinal and Colonic Crypts

The crypt number was defined as the total number of crypts per circumference and was determined by counting the number from crypts found in two to three transverse sections of three mice. For the purpose of identifying the small intestinal crypts, the presence of Paneth cells defined the crypts of mature mice, and clear epithelial invaginations into the mucosa defined the crypts of neonatal and infant mice. We counted a crypt undergoing cleavage, i.e., "crypt fission" or "branching", as two crypts.

Morphologically, apoptosis was defined as the presence of an apoptotic body. This definition correlated well with one that relied on immunohistochemical staining of active caspase 3 (*17*). To quantify the extent of apoptosis, we used two different scoring systems: scoring the number of crypts (as a percentage) containing one or more active caspase 3-positive cells per circumference, and scoring the mean number of apoptotic cells per crypt. However, the extent of apoptosis in the small intestine of 1-day-old mice was scored as the mean number of active caspase 3-positive cells per circumference in the transverse sections, because crypts had not yet formed. The same scoring systems were used to quantify the number of p53-positive crypts (as a percentage) and the mean number of p53-positive cells per crypt. All scoring was performed without knowing whether the mice had been irradiated.

Statistical Analysis

Data are expressed as means ± SEM. Each experiment used three mice. The Student's t test ($P < 0.05$) was used to determine whether experimental values differed significantly between two groups.

RESULTS

Normal Development of Crypts in the Small Intestine and Colon

We first examined the development of intestinal crypts, focusing on morphology and the number of crypts. Plots of the number of crypts present as a function of time and examples of crypt cells expressing Ki-67, reflecting active phases of the cell cycle, are shown in Fig. 1. Supplementary Fig. S1 shows micrographs that document the developmental changes occurring in the anatomical structures of normal small intestinal and colonic crypts between 1 day and 7 weeks postpartum.

1. Small intestine

In the small intestine at 1 day postpartum, invaginating clusters of epithelial cells could be found, but crypts had not yet formed. Morphologically apparent crypts were identified in the proximal region between 4 days and 1 week postpartum and were found next in the middle region and finally in the distal region (Fig. 1A). Then the size and number of crypts increased rapidly (with occasional crypt fission) until 4 weeks postpartum when morphologically mature crypts appeared (Fig. 1A and Supplementary Fig. S1). The number of crypts was nearly constant thereafter (Fig. 1A). Goblet cells were observed 1 day postpartum in the distal region, and Paneth cells, located at the bottom of crypts, developed 1 to 2 weeks postpartum (Supplementary Fig. S1).

At 1 day postpartum, Ki-67 expression was observed in the nuclei of clustered epithelial cells, presumably indicating crypt formation. At 2 weeks postpartum, Ki-67 staining was uniform within a crypt, i.e., was independent of cell position. By 7 weeks postpartum, cells in the proliferative zone (above cell position 4) were most heavily stained (Fig. 1C), as has been reported previously (*18, 19*).

2. Colon

Crypt-like structures were observed at 1 day postpartum (Fig. 1B and Supplementary Fig. S1). Crypt

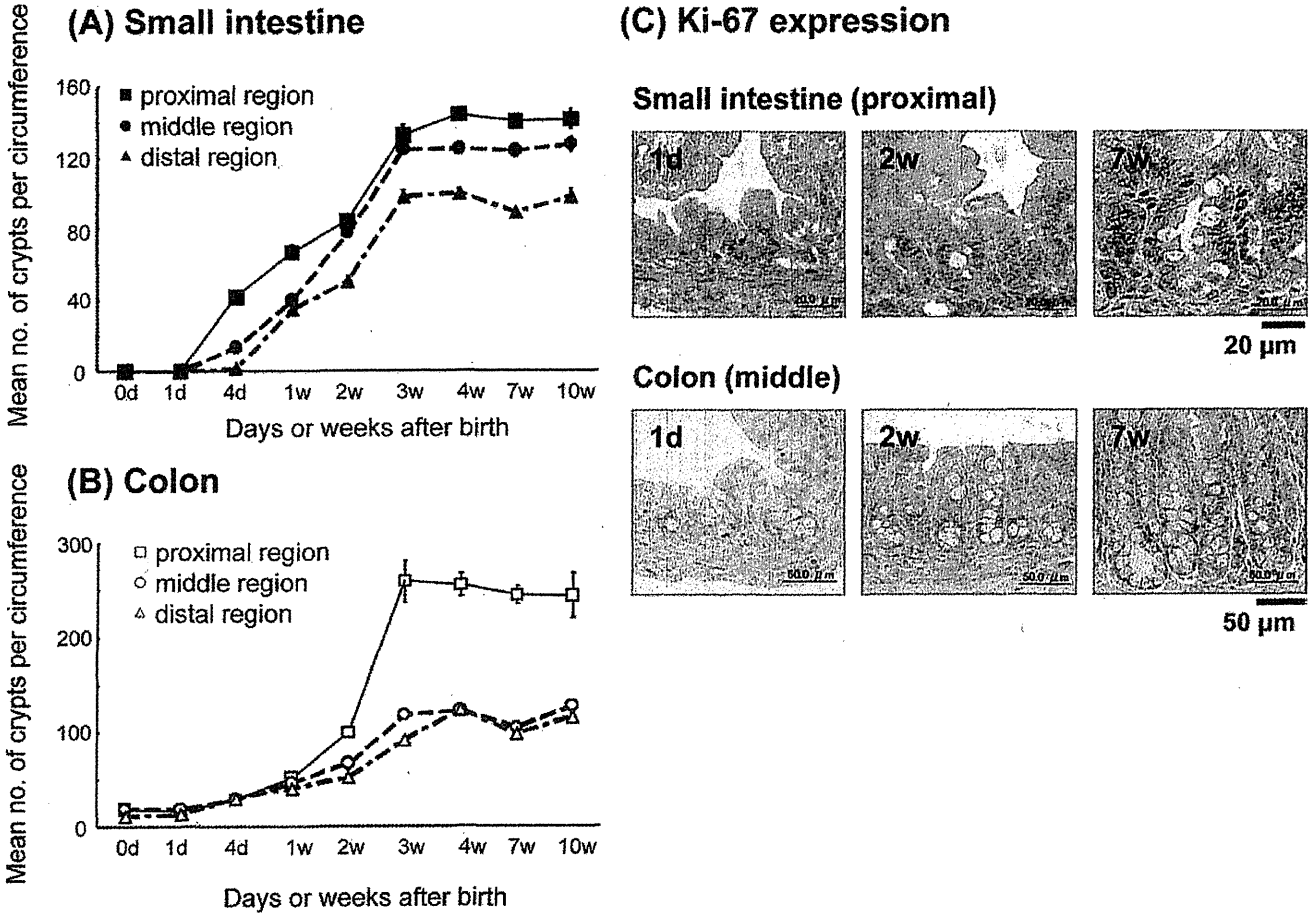

FIG. 1. Developmental changes in the mean number of crypts per circumference for the proximal, middle and distal regions of the small intestine (panel A) and the colon (panel B). Data are reported as means ± SEM. Each experiment used three mice. Panel C: Photomicrographs of Ki-67-stained sections of the small intestine and colon of 1-day-old (1d), 2-week-old (2w) and 7-week-old (7w) mice.

number and size increased with age until 3 to 4 weeks postpartum and were accompanied by frequent crypt fission. Morphologically mature crypts appeared 4 weeks postpartum. The proximal region contained approximately twice as many crypts as did the middle and distal regions (Fig. 1B). Goblet cells developed during the fetal stage (data not shown), which was much earlier than in the small intestine (Supplementary Fig. S1). Ki-67-positive cells were located in the basal one-half to two-thirds of the crypt regardless of age, which was distinctly different from what was seen in the small intestine (Fig. 1C).

Radiation-Induced Apoptosis in Small Intestinal and Colonic Crypts

We next analyzed radiation-induced apoptosis in mice exposed to 2 Gy at 1 day, 2 weeks and 7 weeks postpartum as representatives of neonates with immature or undifferentiated crypts, infants with active proliferative crypts, and adults with a steady number of crypts maintained, respectively (Fig. 1). The dose of 2 Gy was selected based on evidence that the apoptosis in response to ionizing radiation saturates at 1 Gy (*25*). Apoptotic cells were defined as those containing apoptotic bodies and strongly staining for active caspase 3 (*17*). The age and region dependences of the apoptotic response in these mice are shown in Figs. 2, 3 and 4.

1. Small intestine

For mice irradiated at 7 weeks postpartum, apoptosis of crypt cells occurred in two waves (Figs. 2A and 3A). The first wave peaked 3 h after irradiation, as reported previously (*17*), followed by a rapid decrease. The percentage of apoptotic crypts in the first wave was greater than 75% in all regions of the small intestine (Figs. 2A and 4A), and the average number of apoptotic cells was two per crypt (Fig. 3A). The second wave arose thereafter, and its peak level persisted until 48 h. From 10% to 20% of the crypts exhibited apoptosis (Fig. 2A). There were no clear differences among the temporal patterns of the proximal, middle and distal regions (Figs. 2A and 3A). The second apoptotic wave might

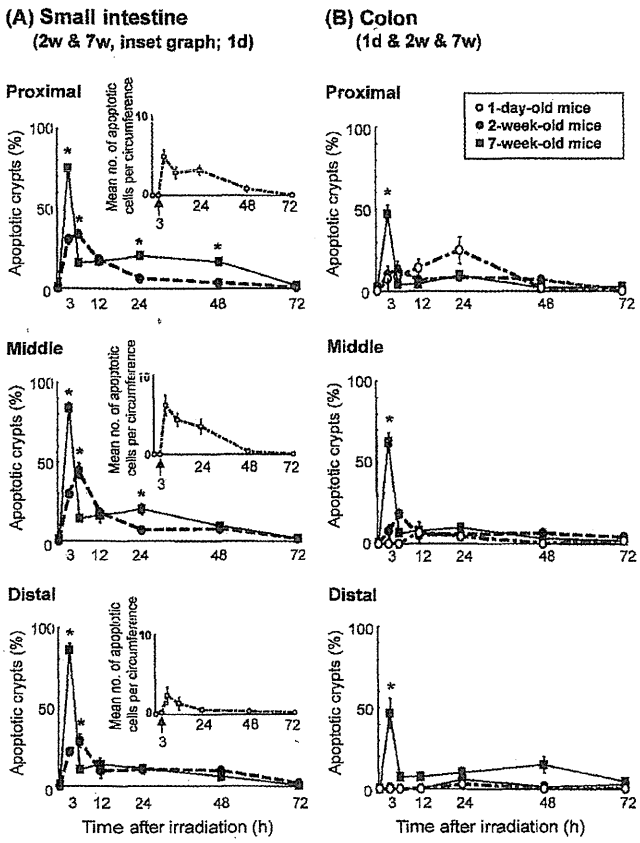

FIG. 2. Percentage of apoptotic crypts as a function of time for the proximal, middle and distal regions of the small intestine (panel A) and the colon (panel B) of mice irradiated at 1 day (1d), 2 weeks (2w) and 7 weeks (7w) postpartum. The inset is a plot of the mean number of apoptotic cells per circumference for 1-day-old irradiated mice. All data are reported as means ± SEM. Each experiment used three mice. For the data points for 2- and 7-week-old mice labeled with an asterisk (*), $P < 0.05$.

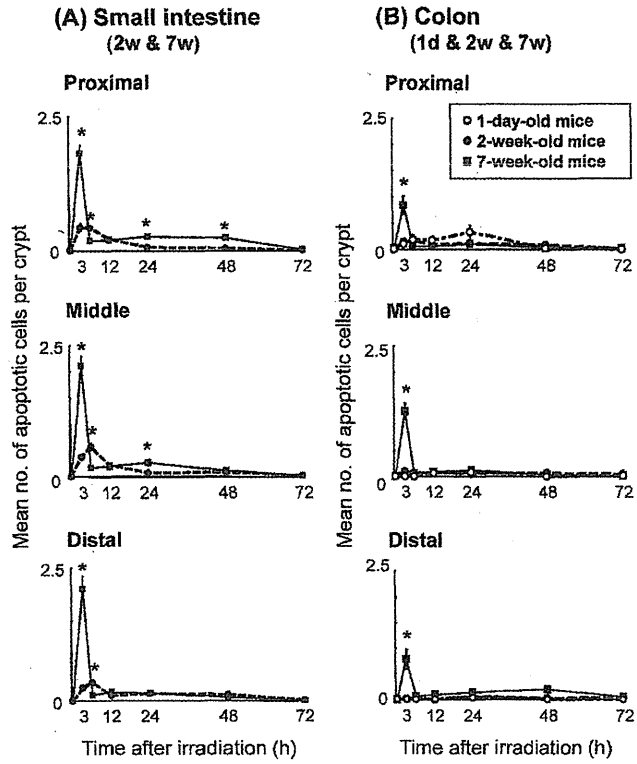

FIG. 3. Mean number of apoptotic cells per crypt as a function of time for the proximal, middle and distal regions of the small intestine of mice irradiated 2 weeks (2w) and 7 weeks (7w) postpartum (panel A) and the colon of mice irradiated 1 day (1d), 2 weeks (2w), and 7 weeks (7w) postpartum (panel B). All data are reported as means ± SEM. Each experiment used three mice. For the data points for 2- and 7-week-old mice labeled with an asterisk (*), $P < 0.05$.

have been the result of a delayed mitotic crisis involving cells that escaped apoptosis during the first wave but then reached the G_2/M checkpoint (*12*).

Compared with the results for 7-week-old mice, the percentage of apoptotic small intestinal crypts in 2-week-old mice at 3 h postirradiation was significantly lower (approximately 20% to 30%; $P < 0.05$; Figs. 2A and 4A). The peak of the first wave occurred 6 h postirradiation, and the average numbers of apoptotic cells per crypt were 0.4, 0.6 and 0.3 for the proximal, middle and distal regions, respectively (Fig. 3A). Only the crypts of the distal region were involved in the second wave of apoptosis (Fig. 2A).

Because no small intestinal crypts were found before the first postpartum day, for the tissues of 1-day-old mice, we used the mean number of apoptotic cells per circumference as a measure of apoptosis. We did not observe any apoptotic cells 3 h after irradiation, instead finding that the maximum apoptosis index occurred at 6 h and persisted until 24 h (Figs. 2A inset and 4A). The mean numbers of apoptotic cells per circumference at 6 h postirradiation were 4.8, 6.2 and 2.3 for the proximal, middle and distal regions, respectively (Fig. 2A insets). At 1 day postpartum, there were approximately 300 to 400 epithelial cells per circumference, which means that approximately 1% of the epithelial cells were very radiosensitive.

2. *Colon*

For 7-week-old mice, the apoptotic response peaked sharply 3 h postirradiation and was followed by a smaller broad response between 24 and 48 h (Figs. 2B, 3B and 4B). Fewer apoptotic cells were found in colonic crypts than in small intestinal crypts (Fig. 3B), as reported previously (*20*). The percentage of apoptotic crypts for the first wave ranged from 47% to 63%, and the average was slightly more than 0.8 apoptotic cell per crypt (Fig. 2B). Conversely, the apoptosis index of colonic crypts of mice irradiated 2 weeks postpartum was much lower, and the maximum values observed for crypts in the proximal and middle regions occurred at 6 h (Fig. 2B). No apoptotic cells were found in the distal region until 12 h postirradiation (Fig. 2B). Colonic cells

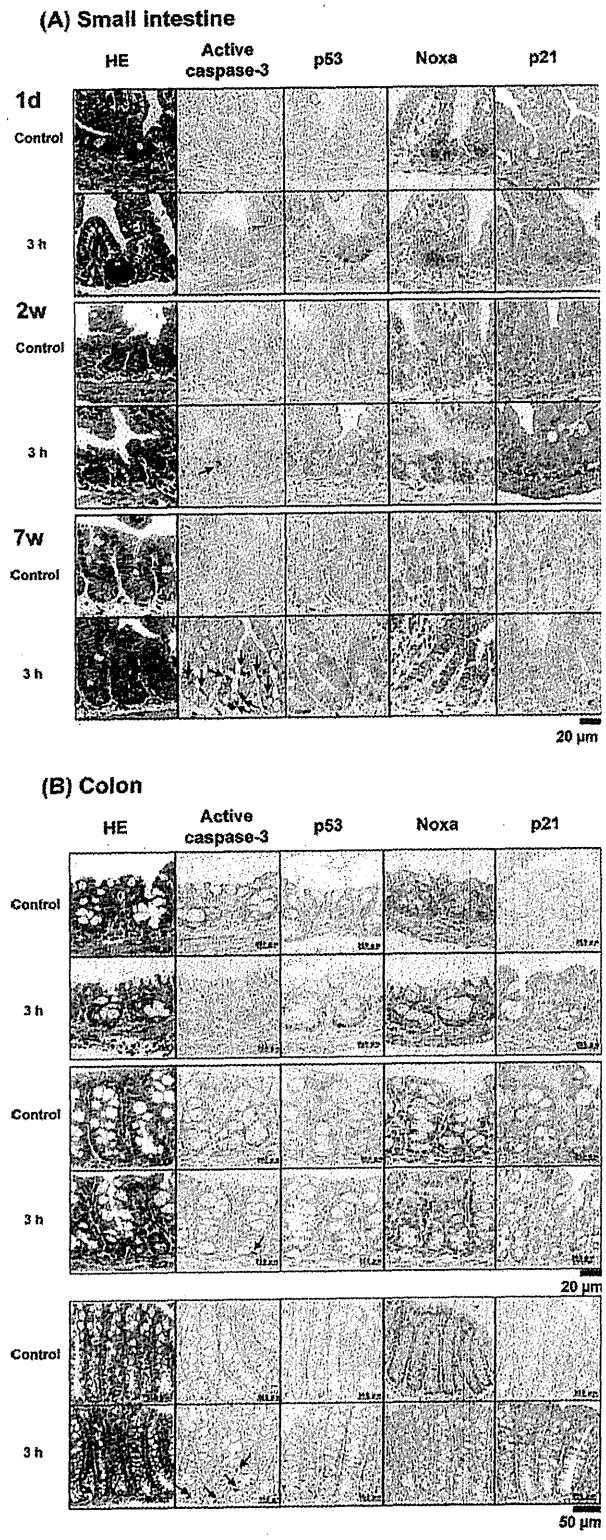

FIG. 4. Photomicrographs of small intestinal (panel A) and colonic (panel B) tissue sections for unirradiated mice and for 1-day-old (1d), 2-week-old (2w) and 7-week-old (7w) mice 3 h after irradiation. From left to right, sections were stained with hematoxylin and eosin or were immunohistologically stained for active caspase 3, p53, Noxa and p21. The arrows point to apoptotic bodies or active caspase 3-positive apoptotic cells.

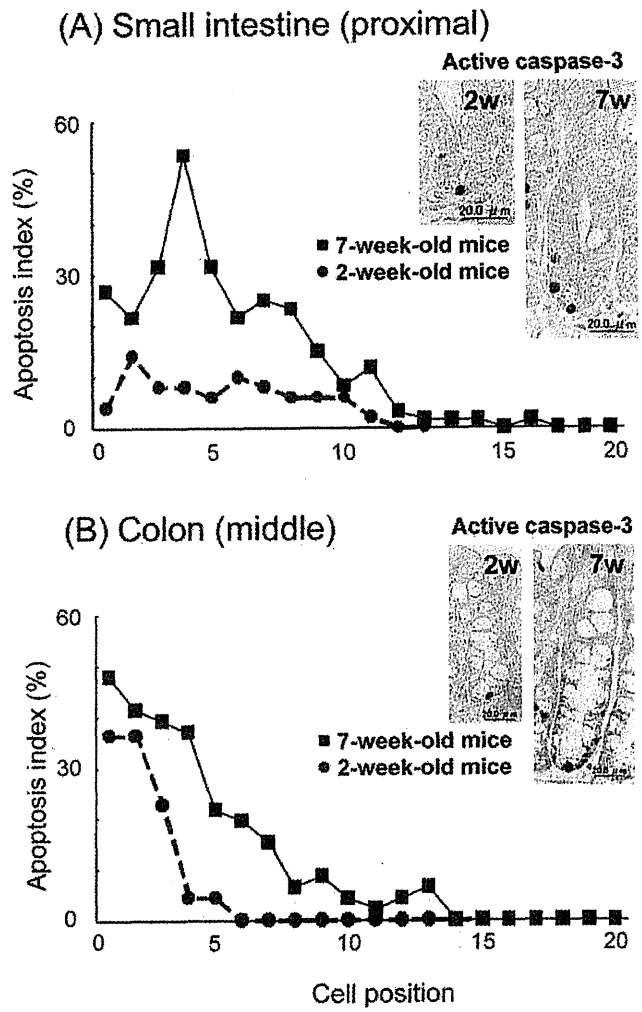

FIG. 5. Age-dependent distribution of apoptotic cells in small intestinal (panel A) and colonic (panel B) crypts. The 2-week-old and 7-week-old mice were irradiated 3 h before being killed. The apoptosis index was calculated using active caspase 3 expression.

irradiated at 1 day postpartum had a unique response to radiation—apoptosis occurred 12 to 24 h postirradiation (Fig. 2B). Moreover, there were regional differences in the mean numbers of apoptotic cells present. The maximum apoptosis index was greater for the proximal colon than for the middle region, and few if any apoptotic crypts were seen in the distal region during the 72-h postirradiation period (Figs. 2B and 3B).

Distribution of Apoptotic Cells in the Small Intestine and Colon

The distribution of apoptotic cells along small intestinal and colonic crypt lengths was determined for 22–50 apoptotic half-crypts of irradiated mice at 2 and 7 weeks of age. The distribution at 3 h postirradiation is shown in Fig. 5. Small intestinal crypts in 7-week-old irradiated mice showed a characteristic peak in the

apoptosis index around cell position 4, a putative stem cell site (*17, 20, 21*). In this study, the small intestinal crypts of 2-week-old mice had smaller apoptosis indices than did those of the adult intestine. Additionally, no specific cell position was associated with a greater radiosensitivity than was any other; instead, similar values for the apoptosis index were broadly distributed as the base of the crypt was approached. Conversely, the frequency of apoptosis in colonic crypts of 7-week-old mice was greatest at cell positions 1–4, the putative stem cell zone (*17, 20*), and declined as the cell position number increased. The colons of 2-week-old mice also had apoptotic cells at the bottom of crypts. These results suggest that normal differentiation of small intestinal cells leads to susceptibility to radiation-induced apoptosis uniquely at cell position 4 during development of the crypt functional architecture, whereas colon cells remain unchanged with regard to cell position-associated radiosensitivity, as indicated by the lack of a difference between 2- and 7-week-old mice.

p53, Noxa and p21 Expression

We examined the age dependence of expression of p53, Noxa and p21, each of which is a crucial determinant of apoptosis (Figs. 4 and 6). Expression of p53 was observed 3 h postirradiation in the cells of the basal half of most intestinal crypts of 7-week-old mice (Fig. 4A and B). Eighty-one percent of the small intestinal crypts were p53 positive, and 100% of the colonic crypts were p53 positive (Fig. 6). Expression of p53 was also high in small intestinal and colonic crypts of irradiated 2-week-old mice, with frequencies of 86% and 95%, respectively. Notably, the apoptosis indices of 2-week-old mice were much lower than those of 7-week-old mice for both the small intestinal and colonic crypts (Fig. 6). Significant p53 expression also occurred in the intestinal crypts of irradiated 1-day-old mice (Fig. 6). Small intestinal cells expressing p53 were clustered in the intervillus region (Fig. 4A); those of the colon were restricted to cells in newly forming crypts (Fig. 4B). It is possible that a link between p53 expression and apoptosis does not exist in the intestine of 1-day- and 2-week-old mice. The levels of p53 expression in the intestinal crypts of 1-day-, 2-week- and 7-week-old mice were negligible at 24 h postirradiation (during the second wave of apoptosis), suggesting that apoptosis was independent of p53 during this time (Fig. 6).

To further characterize the apoptotic response, we immunohistochemically examined the expression of the p53-dependent pro-death factor, Noxa, and pro-survival factor, p21, in the intestinal epithelia of 1-day-old, 2-week-old and 7-week-old irradiated mice. In the small intestine of irradiated 7-week-old mice, Noxa expression increased markedly in cells at positions greater than 4 compared to unirradiated cells, and the expression was

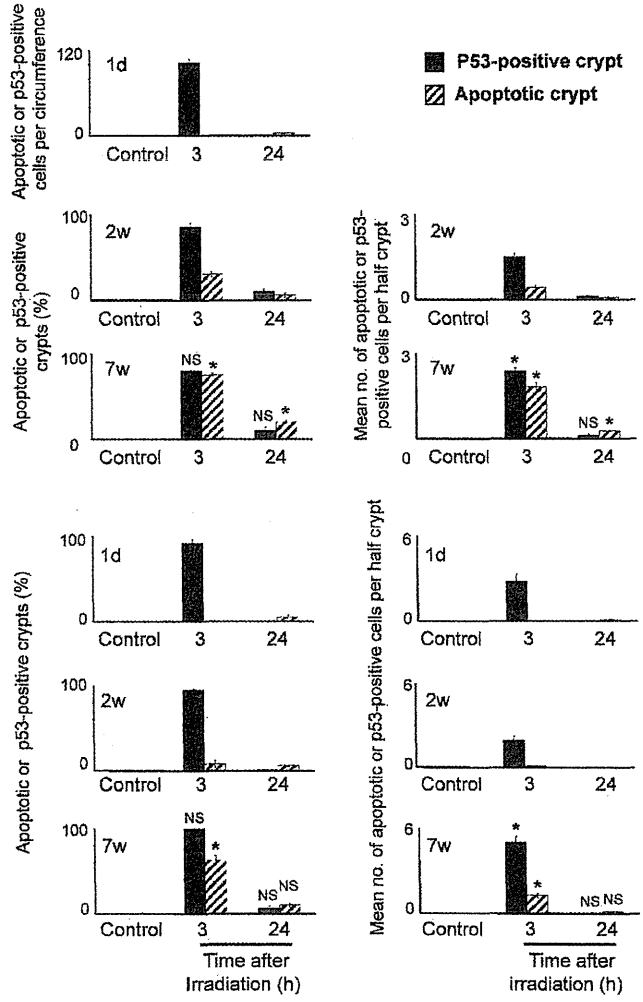

FIG. 6. Percentages of apoptotic crypts and p53-positive crypts (left column) and the mean numbers of apoptotic and p53-positive cells per half crypt (right column) present in tissue sections of the proximal small intestine (panel A) and the colon (panel B) of irradiated mice. For the data for small intestine tissue presented in the right column, mice were 2 weeks old (2w) or 7 weeks old (7w). For 1-day-old (1d) mice, the data for small intestine tissue in the right column are presented as the mean number of apoptotic or p53-positive cells per circumference. Times were 3 h and 24 h after irradiation. The control group was not irradiated. Data are reported as means ± SEM. Each experiment used three mice. For the data points for 7-week-old mice labeled with an asterisk (*), $P < 0.05$ compared to 2-week-old mice.

clearly visible (see dots in Fig. 4A). In irradiated 2-week-old mice, this expression was moderately induced compared to that in 7-week-old mice (Fig. 4A). Unexpectedly, the intervillus region of the small intestine of 1-day-old neonates expressed a substantial amount of Noxa, but the expression level was not influenced by radiation (Fig. 4A). In the colon, Noxa expression was less than that in the small intestine at all ages examined, which may correlate with the relatively low frequency of apoptosis compared to the small intestine (Fig. 4B). The

level of Noxa expression after irradiation in the colonic epithelial cells of 7-week-old mice was increased only slightly. By contrast, in 1-day-old and 2-week-old mice, Noxa expression remained almost unchanged after irradiation (Fig. 4B).

The basal p21 expression levels in the nuclei of small intestinal crypts were the same for 7-week-old mice regardless of whether they had been irradiated. The level of p21 expression increased slightly in cells of 2-week-old irradiated mice. At 1 day postpartum, strong p21 expression was observed both in the nuclei of clustered cells and the cytoplasm of villus and intervillus epithelial cells (Fig. 4A). For the colonic cells of all mice examined, p21 expression was always greater when the mice had been irradiated, as reported previously (*22*). The expression of p21 occurred in the nuclei of cells within the proliferative zone in adult crypts of 7-week-old mice, whereas it occurred throughout crypts of 1-day- and 2-week-old mice (Fig. 4B).

DISCUSSION

For this study, we documented the developmental changes that occur in the small intestine and colon of mice in response to ionizing radiation, an inducer of apoptosis. Unexpectedly, the rapidly growing intestinal epithelial cells of neonatal and infant mice were more radioresistant than were those of adults. Three notable differences were found for how adult and immature crypt cells responded to radiation, as follows. Immature epithelial cells had a delayed first wave of apoptosis in comparison with those of adults. Cells that were extraordinarily susceptible to radiation at mature crypt position 4 were not absorbed in the immature crypt. Especially in neonates, regional differences in radiosensitivities along the intestinal tract were also found—the cells of the small intestinal and colonic distal regions were more radioresistant than were those of the proximal regions.

It has been believed that actively proliferating, immature, undifferentiated epithelial cells are much more sensitive to radiation-induced apoptosis than are differentiated cells (*2–5, 26*). However, as we report here, the intestinal epithelial cells of neonatal and infant mice were more resistant to radiation-induced apoptosis than were those of adults. It has been reported that a dynamic balance between pro-survival and pro-death proteins may determine whether cells undergo apoptosis (*27–29*). In this study, p53 accumulated in irradiated cells regardless of the age of the mouse, whereas there were marked differences in the expression levels of Noxa (a p53-induced pro-apoptosis protein) and p21 (a pro-survival protein) between neonatal, infant and adult intestines. Noxa expression in irradiated adult small intestine increased markedly over the basal level, whereas this was not the case in irradiated neonatal mice. By contrast, p21 expression increased significantly in the cytoplasm and nucleus of neonatal cells in comparison with adult cells. It has been reported that nuclear p21 is necessary for cell cycle arrest (*30, 31*), whereas cytoplasmic p21 inhibits an initiator caspase (*32, 33*). Therefore, after radiation-induced DNA damage, p53 may only marginally induce the expression of pro-apoptosis proteins in neonatal intestinal cells, whereas the cell cycle of neonatal intestinal cells may be arrested efficiently by p53, allowing the cell time to repair its DNA and prevent apoptosis. The balance between cell cycle arrest and apoptosis in response to DNA damage probably changes with development.

Another possible mechanism underlying the radioresistance of neonatal and infant epithelial cells is related to the increased expression of cellular Bcl-2. Bcl-2, which is survival factor, is expressed throughout the intestinal epithelium at embryonic day 14.5 (*34*). At embryonic day 18.5, Bcl-2 expression is restricted to the base of villi; in adult cells, it has been detected in only a small fraction of crypt cells (*11*). Thus the different radiosensitivities of the adult and infant small intestine and colon may be partly explained by their distinctly different Bcl-2 expression profiles (*11, 13, 14*). It was recently found that Wnt/beta-catenin mediates the radioresistance of mouse mammary progenitor cells (*35*). The Wnt signaling pathway is intimately involved in the regulation of intestinal development and maintenance (*36–40*). During the late fetal period, Wnt signaling occurs in newly formed villi and by 3 days postpartum in intervillus cells. After weaning, Wnt activity is confined to the cells of the crypt base (*41*). Therefore, developmental changes in Bcl-2 activity and Wnt signaling may also account in part for radioresistance. Additionally, radioresistance may also be associated with the degree to which cells can repair DNA damage, the rate and mode of stem cell division, and the type and abundance of intestinal microflora present (*42–45*).

Potten has hypothesized that the observed greater resistance to apoptosis by colonic crypts (compared with small intestinal crypts) may account for the greater incidence of colonic carcinoma (*24, 46*). We found here that neonatal and infant intestinal epithelial cells were more resistant to radiation-induced apoptosis than were those of adults. Temporally, $Apc^{Min/+}$ mice, a murine model of human familial adenomatous polyposis, have been shown to be most sensitive to intestinal tumor induction when irradiated at 10 to 12 days of age (*47, 48*). This age-related tumor susceptibility could be explained by a failure of cells with sustained DNA damage to undergo apoptosis and is a possible mechanism carcinogenesis that is consistent with Potten's proposal (*24, 46*).

In conclusion, we demonstrated that, in the developing intestine of C57BL/6J mice, the extent of radiation-induced apoptosis is dependent on age, tissue type and

organ region. Neonatal and infant intestinal epithelial cells were more resistant to radiation-induced apoptosis than were those of adults. When the molecular mechanisms underlying age-related radiosensitivity are better characterized, it may be possible to predict more accurately when children exposed to radiation will develop cancer and use preventive measures to decrease their risk.

SUPPLEMENTARY INFORMATION

Supplementary Fig. S1. Photomicrographs of transverse sections of small intestinal (A) and colonic (B) tissue taken from unirradiated female mice between the ages of 1 day (1d) and 7 weeks postpartum (7w). The arrows labeled A point to clusters of epithelial cells. Arrows labeled B point to crypts undergoing fission. http://dx.doi.org/10.1667/RR1905.1.S1

ACKNOWLEDGMENTS

We thank Drs. K. Yamauchi, Y. Morita, H. Kawame, Y. Kakiuchi and K. Takizawa for helpful comments. We are also greatly thankful to Ms. E. Obara and Y. Amasaki for their technical and secretarial assistance, and to all members of the Division of Animal Facility for help with animal maintenance. This study was financially supported in part by Grants-in-Aid for Scientific Research from the Ministry of Education, Culture, Sports, Science, and Technology, Grants-in-Aid for Cancer Research and Third-Term Comprehensive Strategy for Cancer Control from the Ministry of Health, Labour and Welfare, and a grant from the Long-range Research Initiative (LRI) of the Japan Chemical Industry Association (JCIA).

Received: June 23, 2009; accepted: October 14, 2009; published online: December 8, 2009

REFERENCES

1. J. Bergonie and L. Tribondeau, Interpretation of some results from radiotherapy and an attempt to determine a rational treatment technique. 1906. *Yale J. Biol. Med.* **76**, 181–182 (2003). [originally published in *C. R. Seances Acad. Sci.* **143**, 983–985 (1906)]
2. I. Ferrer, The effect of cycloheximide on natural and X-ray-induced cell death in the developing cerebral cortex. *Brain Res.* **588**, 351–357 (1992).
3. G. C. Gobe, R. A. Axelsen, B. V. Harmon and D. J. Allan, Cell death by apoptosis following X-irradiation of the foetal and neonatal rat kidney. *Int. J. Radiat. Biol.* **54**, 567–576 (1988).
4. S. S. Fred and W. W. Smith, Radiation sensitivity and proliferative recovery of hemopoietic stem cells in weanling as compared to adult mice. *Radiat. Res.* **32**, 314–326 (1967).
5. Y. Shimada, J. Yasukawa-Barnes, R. Y. Kim, M. N. Gould and K. H. Clifton, Age and radiation sensitivity of rat mammary clonogenic cells. *Radiat. Res.* **137**, 118–123 (1994).
6. G. B. Gerber and J. Maes, Stem cell kinetics in spleen and bone marrow after single and fractionated irradiation of infant mice. *Radiat. Environ. Biophys.* **18**, 249–256 (1980).
7. A. G. Renehan, C. Booth and C. S. Potten, What is apoptosis, and why is it important? *Br. Med. J.* **322**, 1536–1538 (2001).
8. A. J. Watson and D. M. Pritchard, Lessons from genetically engineered animal models. VII. Apoptosis in intestinal epithelium: lessons from transgenic and knockout mice. *Am. J. Physiol. Gastrointest. Liver Physiol.* **278**, G1–G5 (2000).
9. A. R. Clarke, S. Gledhill, M. L. Hooper, C. C. Bird and A. H. Wyllie, p53 dependence of early apoptotic and proliferative responses within the mouse intestinal epithelium following gamma-irradiation. *Oncogene* **9**, 1767–1773 (1994).
10. A. J. Merritt, C. S. Potten, C. J. Kemp, J. A. Hickman, A. Balmain, D. P. Lane and P. A. Hall, The role of p53 in spontaneous and radiation-induced apoptosis in the gastrointestinal tract of normal and p53-deficient mice. *Cancer Res.* **54**, 614–617 (1994).
11. A. J. Merritt, C. S. Potten, A. J. Watson, D. Y. Loh, K. Nakayama, K. Nakayama and J. A. Hickman, Differential expression of bcl-2 in intestinal epithelia. Correlation with attenuation of apoptosis in colonic crypts and the incidence of colonic neoplasia. *J. Cell Sci.* **108**, 2261–2271 (1995).
12. A. J. Merritt, T. D. Allen, C. S. Potten and J. A. Hickman, Apoptosis in small intestinal epithelial from p53-null mice: evidence for a delayed, p53-independent G_2/M-associated cell death after gamma-irradiation. *Oncogene* **14**, 2759–2766 (1997).
13. K. P. Hoyes, W. B. Cai, C. S. Potten and J. H. Hendry, Effect of bcl-2 deficiency on the radiation response of clonogenic cells in small and large intestine, bone marrow and testis. *Int. J. Radiat. Biol.* **76**, 1435–1442 (2000).
14. D. M. Pritchard, C. S. Potten, S. J. Korsmeyer, S. Roberts and J. A. Hickman, Damage-induced apoptosis in intestinal epithelia from bcl-2-null and bax-null mice: investigations of the mechanistic determinants of epithelial apoptosis in vivo. *Oncogene* **18**, 7287–7293 (1999).
15. D. M. Pritchard, C. Print, L. O'Reilly, J. M. Adams, C. S. Potten and J. A. Hickman, Bcl-w is an important determinant of damage-induced apoptosis in epithelia of small and large intestine. *Oncogene* **19**, 3955–3959 (2000).
16. K. Martin, C. S. Potten and T. B. Kirkwood, Age-related changes in irradiation-induced apoptosis and expression of p21 and p53 in crypt stem cells of murine intestine. *Ann. NY Acad. Sci.* **908**, 315–318 (2000).
17. E. Marshman, P. D. Ottewell, C. S. Potten and A. J. Watson, Caspase activation during spontaneous and radiation-induced apoptosis in the murine intestine. *J. Pathol.* **195**, 285–292 (2001).
18. W. S. el-Deiry, T. Tokino, T. Waldman, J. D. Oliner, V. E. Velculescu, M. Burrell, D. E. Hill, E. Healy, J. L. Rees and B. Vogelstein, Topological control of p21WAF1/CIP1 expression in normal and neoplastic tissues. *Cancer Res.* **55**, 2910–2919 (1995).
19. C. S. Potten, Stem cells in gastrointestinal epithelium: numbers, characteristics and death. *Phil. Trans. R. Soc. Lond. B Biol. Sci.* **353**, 821–830 (1998).
20. C. S. Potten and H. K. Grant, The relationship between ionizing radiation-induced apoptosis and stem cells in the small and large intestine. *Br. J. Cancer* **78**, 993–1003 (1998).
21. C. S. Potten, Radiation, the ideal cytotoxic agent for studying the cell biology of tissues such as the small intestine. *Radiat. Res.* **161**, 123–136 (2004).
22. J. W. Wilson, D. M. Pritchard, J. A. Hickman and C. S. Potten, Radiation-induced p53 and p21WAF-1/CIP1 expression in the murine intestinal epithelium: apoptosis and cell cycle arrest. *Am. J. Pathol.* **153**, 899–909 (1998).
23. C. S. Potten, C. Booth and D. Hargreaves, The small intestine as a model for evaluating adult tissue stem cell drug targets. *Cell Prolif.* **36**, 115–129 (2003).
24. E. Marshman, C. Booth and C. S. Potten, The intestinal epithelial stem cell. *Bioessays* **24**, 91–98 (2002).
25. C. S. Potten, A. Merritt, J. Hickman, P. Hall and A. Faranda, Characterization of radiation-induced apoptosis in the small intestine and its biological implications. *Int. J. Radiat. Biol.* **65**, 71–78 (1994).
26. I. Szumiel, Ionizing radiation-induced cell death. *Int. J. Radiat. Biol.* **66**, 329–341 (1994).

27. P. Fei, E. J. Bernhard and W. S. El-Deiry, Tissue-specific induction of p53 targets in vivo. *Cancer Res.* **62**, 7316–7327 (2002).

28. S. N. Willis and J. M. Adams, Life in the balance: how BH3-only proteins induce apoptosis. *Curr. Opin. Cell Biol.* **17**, 617–625 (2005).

29. J. Yu and L. Zhang, The transcriptional targets of p53 in apoptosis control. *Biochem. Biophys. Res. Commun.* **331**, 851–858 (2005).

30. F. Goubin and B. Ducommun, Identification of binding domains on the p21Cip1 cyclin-dependent kinase inhibitor. *Oncogene* **10**, 2281–2287 (1995).

31. C. J. Sherr and J. M. Roberts, Inhibitors of mammalian G1 cyclin-dependent kinases. *Genes Dev.* **9**, 1149–1163 (1995).

32. S. Q. Xu and W. S. El-Deiry, p21(WAF1/CIP1) inhibits initiator caspase cleavage by TRAIL death receptor DR4. *Biochem. Biophys. Res. Commun.* **269**, 179–190 (2000).

33. M. Asada, T. Yamada, H. Ichijo, D. Delia, K. Miyazono, K. Fukumuro and S. Mizutani, Apoptosis inhibitory activity of cytoplasmic p21(Cip1/WAF1) in monocytic differentiation. *EMBO J.* **18**, 1223–1234 (1999).

34. D. V. Novack and S. J. Korsmeyer, Bcl-2 protein expression during murine development. *Am. J. Pathol.* **145**, 61–73 (1994).

35. W. A. Woodward, M. S. Chen, F. Behbod, M. P. Alfaro, T. A. Buchholz and J. M. Rosen, WNT/beta-catenin mediates radiation resistance of mouse mammary progenitor cells. *Proc. Natl. Acad. Sci. USA* **104**, 618–623 (2007).

36. D. Pinto, A. Gregorieff, H. Begthel and H. Clevers, Canonical Wnt signals are essential for homeostasis of the intestinal epithelium. *Genes Dev.* **17**, 1709–1713 (2003).

37. J. Hoffman, F. Kuhnert, C. R. Davis and C. J. Kuo, Wnts as essential growth factors for the adult small intestine and colon. *Cell Cycle* **3**, 554–557 (2004).

38. F. Kuhnert, C. R. Davis, H. T. Wang, P. Chu, M. Lee, J. Yuan, R. Nusse and C. J. Kuo, Essential requirement for Wnt signaling in proliferation of adult small intestine and colon revealed by adenoviral expression of Dickkopf-1. *Proc. Natl. Acad. Sci. USA* **101**, 266–271 (2004).

39. M. van de Wetering, E. Sancho, C. Verweij, W. de Lau, I. Oving, A. Hurlstone, K. van der Horn, E. Batlle, D. Coudreuse and H. Clevers, The beta-catenin/TCF-4 complex imposes a crypt progenitor phenotype on colorectal cancer cells. *Cell* **111**, 241–250 (2002).

40. V. Korinek, N. Barker, P. Moerer, E. van Donselaar, G. Huls, P. J. Peters and H. Clevers, Depletion of epithelial stem-cell compartments in the small intestine of mice lacking Tcf-4. *Nat. Genet.* **19**, 379–383 (1998).

41. B. M. Kim, J. Mao, M. M. Taketo and R. A. Shivdasani, Phases of canonical Wnt signaling during the development of mouse intestinal epithelium. *Gastroenterology* **133**, 529–538 (2007).

42. I. L. Steffensen, H. A. Schut, J. E. Paulsen, A. Andreassen and J. Alexander, Intestinal tumorigenesis in multiple intestinal neoplasia mice induced by the food mutagen 2-amino-1-methyl-6-phenylimidazo[4,5-b]pyridine: perinatal susceptibility, regional variation, and correlation with DNA adducts. *Cancer Res.* **61**, 8689–8696 (2001).

43. C. S. Potten, G. Owen and D. Booth, Intestinal stem cells protect their genome by selective segregation of template DNA strands. *J. Cell Sci.* **115**, 2381–2388 (2002).

44. J. L. Sherley, P. B. Stadler and D. R. Johnson, Expression of the wild-type p53 antioncogene induces guanine nucleotide-dependent stem cell division kinetics. *Proc. Natl. Acad. Sci. USA* **92**, 136–140 (1995).

45. J. R. Merok, J. A. Lansita, J. R. Tunstead and J. L. Sherley, Cosegregation of chromosomes containing immortal DNA strands in cells that cycle with asymmetric stem cell kinetics. *Cancer Res.* **62**, 6791–6795 (2002).

46. C. S. Potten, Y. Q. Li, P. J. O'Connor and D. J. Winton, A possible explanation for the differential cancer incidence in the intestine, based on distribution of the cytotoxic effects of carcinogens in the murine large bowel. *Carcinogenesis* **13**, 2305–2312 (1992).

47. M. Okamoto and H. Yonekawa, Intestinal tumorigenesis in Min mice is enhanced by X-irradiation in an age-dependent manner. *J. Radiat. Res. (Tokyo)* **46**, 83–91 (2005).

48. M. Ellender, J. D. Harrison, R. Kozlowski, M. Szluinska, S. D. Bouffler and R. Cox, *In utero* and neonatal sensitivity of $Apc^{Min/+}$ mice to radiation-induced intestinal neoplasia. *Int. J. Radiat. Biol.* **82**, 141–151 (2006).

Biochemical and Biophysical Research Communications 392 (2010) 140–144

Contents lists available at ScienceDirect

Biochemical and Biophysical Research Communications

journal homepage: www.elsevier.com/locate/ybbrc

Specific amino acid residues are involved in substrate discrimination and template binding of human REV1 protein

Jinlian Piao, Yuji Masuda *, Kenji Kamiya *

Research Institute for Radiation Biology and Medicine, Hiroshima University, 1-2-3 Kasumi, Minami-ku, Hiroshima 734-8553, Japan

ARTICLE INFO

Article history:
Received 9 December 2009
Available online 6 January 2010

Keywords:
Y-family DNA polymerase
Deoxycytidyl transferase
Kinetic parameter

ABSTRACT

REV1 is a member of the Y-family DNA polymerases, but is atypical in utilizing only dCTP with a preference for guanine (G) as the template. Crystallography of the REV1–DNA–dCTP ternary complex has revealed a unique mechanism by which template G is evicted from the DNA helix and incoming dCTP is recognized by an arginine residue in an α-loop, termed the N-digit. To better understand functions of its individual amino acid residues, we made a series of mutant human REV1 proteins. We found that R357 and L358 play vital roles in template binding. Furthermore, extensive mutation analysis revealed a novel function of R357 for substrate discrimination, in addition to previously proposed specific interaction with incoming dCTP. We found that the binding pocket for dCTP of REV1 has also significant but latent affinity for dGTP. The results suggest that the positive charge on R357 could prevent interaction with dGTP. We propose that both direct and indirect mechanisms mediated by R357 ensure specificity for dCTP.

© 2010 Elsevier Inc. All rights reserved.

Introduction

Accurate DNA replication is crucial for living organisms. Replicases, which are responsible for genomic duplication, are high-fidelity DNA polymerases whose fidelity is achieved by two characteristics [1]. One is high nucleotide selectivity. The correct Watson–Crick base pair is able to enter into binding pockets without steric clashes. The other is proof reading activity catalyzed by intrinsic 3′ exonuclease. As a consequence of these properties, replicases can not extend primer termini beyond damage bases, resulting in replication blocks [1].

Cells also have another class of DNA polymerases [2], the Y-family members pol η, ι, and κ, which are able to extend primer ends beyond damage bases [3,4]. Consequently, stalled DNA synthesis can be restored. The molecular mechanism allowing incorporation of a deoxyribonucleotide opposite a damaged template is of great interest and there is evidence that a lack of proofreading activity and lower nucleotide selectivity are involved [1], even though DNA polymerase η an κ also utilize Watson–Crick base pairs for nucleotide selection [4]. DNA polymerase ι has an additional property, which is utilization of Hoogsteen base pairs for nucleotide selection, to bypass damage bases [4].

REV1 is a well-conserved Y-family polymerase in eukaryotes. Despite belonging with polymerase family, this enzyme is able to utilize only dCTP as the dNTP source for its deoxycytidyl transferase activity [5]. dCMP is thereby incorporated opposite template G, various DNA lesions, and also opposite templates A, T, and C [6]. Steady-state kinetic studies have demonstrated that templates G and apurinic/apyrimidinic (AP) site are good substrates for the transferase reactions [7–10] and crystallography of yeast and human REV1 has revealed unique mechanisms for recognition of template G and incoming dCTP [11,12]. REV1 has a loose α-loop structure, termed the N-digit, and another structure, named the G-loop, which are conserved in the REV1 family, but not other Y polymerase members. The template G and incoming dCTP do not pair with each other. Instead, the template G is evicted from the DNA helix and interacts with amino acids in the G-loop, and incoming dCTP forms a hydrogen bond with an arginine residue in the N-digit [11,12].

In the present study, we made a series of mutant human REV1 proteins to analyse which amino acid residues are involved in substrate discrimination and template binding. The results suggested that the conserved amino acid residues in the N-digit play crucial roles in bypass synthesis of damaged templates. Together with information from the crystal structure, we discuss novel functions of the N-digit for substrate discrimination and template binding of human REV1 protein.

Abbreviations: AP, apurinic/apyrimidinic; F, tetrahydrofuran; 8oxG, 8-oxoguanine.

* Corresponding authors. Fax: +81 82 257 5843 (Y. Masuda); +81 82 257 5844 (K. Kamiya).

E-mail addresses: piao@hiroshima-u.ac.jp (J. Piao), masudayu@hiroshima-u.ac.jp (Y. Masuda), kkamiya@hiroshima-u.ac.jp (K. Kamiya).

0006-291X/$ - see front matter © 2010 Elsevier Inc. All rights reserved.
doi:10.1016/j.bbrc.2009.12.167

Materials and methods

Proteins. Truncated human *REV1* genes were made by PCR with introduction of an NdeI site at the initiation codon, and inserted into the NdeI site of pET15b. In some cases, the coding region of the resulting plasmids was subcloned into an XbaI site of pBAD22A in which gene expression was induced by arabinose [13]. All proteins were purified as his-tagged fusion proteins, as described previously [13,14] by sequential chromatography using HiTrap Chelating and Superdex 200 columns (GE Healthcare). Protein concentrations were determined by BIO-RAD protein assay using BSA (BIO-RAD) as the standard.

Transferase assay. Oligonucleotide templates 5′-CTCGTCAGCAT CTTCAXCATACAGTCAGTG-3′ [X = G, A, T, C, tetrahydrofuran (F) and 8-oxoguanine (8oxG)] and the primer 5′-CACTGACTGTATG-3′ were purchased. The latter was labeled using polynucleotide kinase (New England BioLabs) and [γ-^{32}P] ATP (GE Healthcare), and annealed to the templates. The standard reaction mixture (25 μl) contained 50 mM Tris–HCl buffer, pH 8.0, 2 mM $MgCl_2$, 25 mM $(NH_4)_2SO_4$, 0.1 mg/ml BSA, 5 mM dithiothreitol, 0.1 mM dNTP, 100 nM primer-template and 1 μl of protein sample, diluted with buffer (50 mM HEPES [4-(2-hydroxyethyl)-1-piperazineethanesulfonic acid]–NaOH, pH 7.5, 10% glycerol, 10 mM β-mercaptoethanol, 500 mM NaCl, and 0.1 mg/ml BSA) as indicated. After incubation at 30 °C for the indicated time, reactions were terminated with 10 μl of stop solution (30 mM EDTA/94% formamide/0.05% bromophenol blue/0.05% xylene cyanole) and products were resolved on 20% polyacrylamide gels containing 8 M urea and autoradiographed at −80 °C. The amount of DNA present in each band was quantified using a Bio-Imaging Analyzer BAS2000 (Fuji Photo Film Co., Ltd.).

Results

To determine the minimum region required for the deoxycytidyl transferase activity of REV1 protein, we made and purified a series of deletion mutants as his-tagged fusion proteins at the N-termini. The transferase activities of the truncated proteins were measured by the standard assay containing 0.1 mM dCTP and 100 nM primer-template with template G. The results revealed that the minimum region exhibiting equivalent activity with full length REV1 was the portion between amino acid residues 341 and 829 (Fig. 1A). Further truncation of 29 amino acid residues at the N-terminal or 10 amino acid residues at the C-terminal reduced the transferase activity to less than 1% of the wild-type value. The kinetic parameters of the deletion mutant consisting of the minimum region, REV1$^{(341–829)}$ indicated that the activity was in fact slightly higher than that of the full-length protein (Table 1). We considered that the difference is due to the instability of the full-length protein [13] but the properties were found to be essentially identical (Table 1). We concluded that the REV1$^{(341–829)}$ is the necessary and sufficient region for the transferase activity, which is slightly shorter than that previously reported [12].

The N-terminal 29 amino acid residues of REV1$^{(341–829)}$, which is the portion of the α-helix structure named the N-digit [12], proved essential for transferase activity (Fig. 1A). The region is well conserved in REV1 proteins of various species (Fig. 1B). To determine the functional role of the conserved amino acid residues, we first replaced each of the most conserved five amino acid residues of REV1$^{(341–829)}$ with alanines (Fig. 1B). The mutant proteins F348A, S356A, R357A, L358A, and H359A were produced in *E. coli*, and purified with the same qualities (Fig. 2).

Then, we determined kinetic parameters of these mutants using template G, and 8oxG and F as model substrates for damaged bases. The replacement of F348 with alanine did not greatly affect the dCMP transferase activity (Table 2). In contrast, replacements in the conserved SRLH motif markedly reduced the activity

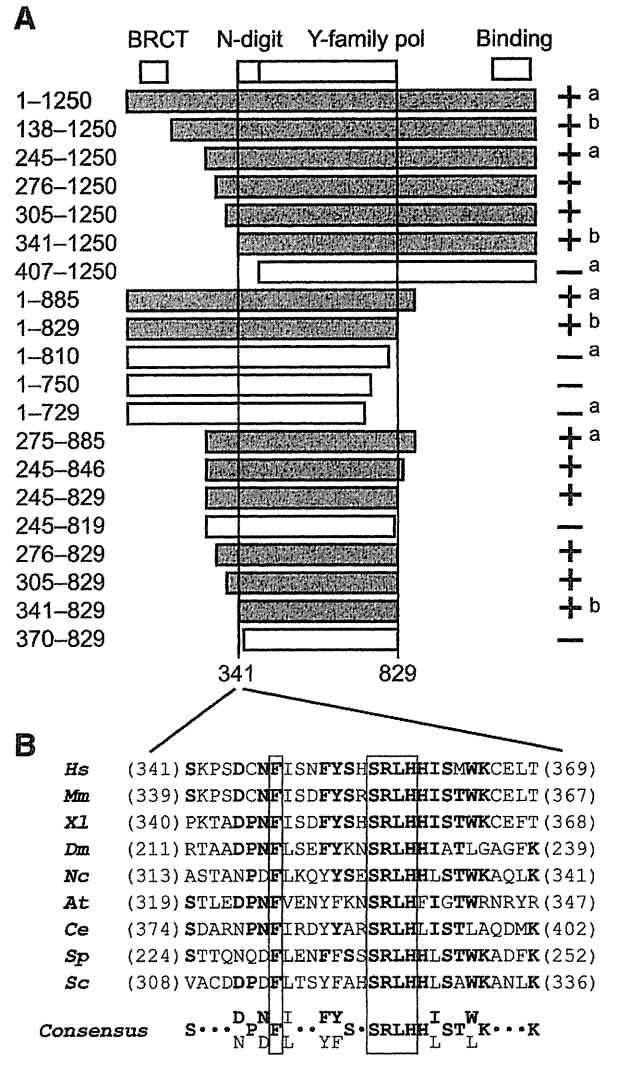

Fig. 1. Deletion analysis of human REV1 protein. (A) Schematic representation of deletion mutants of REV1 protein with their activities. Numbers indicate corresponding amino acid residues of deletion mutants. BRCT, BRCA1 C terminal (BRCT) domain; Y-family pol, conserved region among the family. Binding, binding domain with REV7 and other Y-family DNA polymerases, polη, ι, and κ. + and gray boxes represent activity more than 50% of the full length level. – and open boxes represent transferase activity less than 1% of the full length level. a, data from Ref. [13]. b, data from Ref. [14]. (B) Alignment of amino acid sequences between 341–369 of human REV1 (*Hs*) and corresponding regions of *Mm* (*Mus musculus*), *Xl* (*Xenopus laevis*), *Dm* (*Drosophila melanogaster*), *Nc* (*Neurospora crassa*), *At* (*Arabidopsis thaliana*), *Ce* (*Caenorhabditis elegans*), *Sp* (*Schizosaccharomyces pombe*), and *Sc* (*Saccharomyces cerevisiae*). The conserved amino acids residues are shown in bold letters and the most conserved ones are boxed.

(Table 2). In particular, replacement of R357 and L358 strongly reduced k_{cat} and increased K_M values with the three templates (Table 2). To test the possibility that the defect might be attributed, at least in part, to lowered affinities to template DNA, we determined K_M values. Expectedly, the result showed that K_M values for the three templates with these mutants were much higher than that for wild-type (Table 3), suggesting vital roles of R357 and L358 residues in DNA binding. Interestingly, with L358A the defects in template G and template 8oxG were much more severe than that for the template AP site, whereas with R357A the K_M values were similarly increased with all the three templates (Table 3). This suggested that R357 and L358 residues play distinct roles in DNA binding (see Discussion).

We found that one mutant, R357A exhibited a drastic change for dNTP discrimination on reactions with template G (Fig. 3),

Table 1
Kinetic analysis of REV1$^{(341-829)}$ for dCMP incorporation with various DNA templates. Kinetic assays were performed for 5 min in 25 μl reaction mixtures using 23 fmol REV1$^{(341-829)}$ and 2.5 pmol of the indicated primer-templates. The AP template contained a tetrahydrofuran as an AP site analog. To determine K_M values for dCTP, its concentrations ranged from 1 to 1000 μM. K_M and k_{cat} were evaluated from the plot of the initial velocity versus the dCTP concentration using a hyperbolic curve-fitting program. Data from two to four independent experiments were plotted together and the correlation coefficients (R^2) were more than 0.97.

Template	REV1[a]			REV1$^{(341-829)}$		
	k_{cat} (s^{-1})	K_M (μM)	k_{cat}/K_M ($s^{-1}M^{-1}$)	k_{cat} (s^{-1})	K_M (μM)	k_{cat}/K_M ($s^{-1}M^{-1}$)
G	0.050	0.54	93000	0.073	0.33	220000
A	0.052	23	2300	0.080	29	2800
T	0.027	180	150	0.062	100	610
C	0.030	170	180	0.058	100	560
AP	0.082	7.6	11000	0.13	11	12000

[a] Data from a Ref. [9].

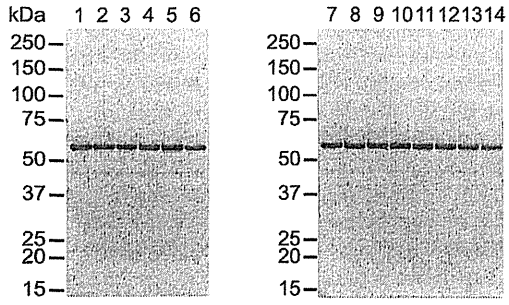

Fig. 2. Sodium dodecyl sulfate–polyacrylamide gel electrophoresis of purified REV1 mutants. The purified proteins (1 μg) were loaded on an 4–20% gradient polyacrylamide gel and stained with Coomassie Brilliant Blue R-250. lane 1, REV1$^{(341-829)}$; lane 2, F348A; lane 3, H359A; lane 4, S356A; lane 5, R357A; lane 6, L358A; lane 7, REV1$^{(341-829)}$; lane 8, R357A; lane 9, R357K; lane 10, R357S; lane 11, R357G; lane 12, R357T; lane 13, R357Q; lane 14, R357M.

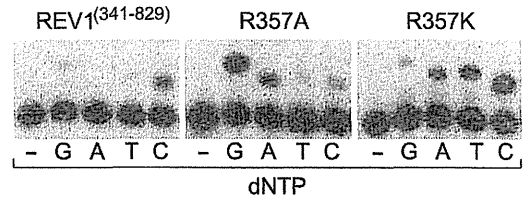

Fig. 3. Altered substrate specificity of R357A and R357K mutants. REV1$^{(341-829)}$ (23 fmol) R357A (26 fmol) or R357K (44 fmol) were incubated under standard reaction conditions with 100 nM of template G and 0.1 mM of each dNTP at 30 °C for 10 min. The reaction products were resolved in 20% polyacrylamide gels containing 8 M urea, and autoradiographed at −80 °C.

the K_M for dCTP being increased 240-fold (Table 4). Surprisingly, the K_M for dGTP, an inappropriate nucleotide, was decreased to 23 μM from 300 μM for the wild-type (Table 4). The efficiencies of dGMP incorporation opposite template G and template 8oxG of the mutant were similar to that for dCTP incorporation opposite template 8oxG of the wild-type (Table 4).

For further analysis of mechanisms of dNTP discrimination by R357, we replaced the arginine residue to lysine, serine, glycine, threonine, glutamine, and methionine. The mutant proteins were purified with equivalent qualities (Fig. 2). Regarding substrate specificity of these mutants under standard assay conditions we found that the properties of R357S, R357G, R357T, R357Q, and R357M were similar to that of R357A having preference for dGTP, while R357K was unique (Fig. 3, data not shown). Consequently, we selected R357K and R357S for further kinetic analysis. The kinetic parameters of the mutant R357S demonstrated similarity to those for R357A, exhibiting preference for dGTP (Table 4). In contrast, R357K retained the preference for dCTP and exhibited slightly higher activities for incorporation of dATP and dTTP on the template G (Table 4).

Table 2
Kinetic analysis of REV1$^{(341-829)}$ and mutants for dCMP incorporation with various DNA templates. Kinetic assays were performed for 5 min in 25 μl reaction mixtures using 2.5 pmol of the indicated primer-templates. The enzyme concentrations ranged from 44 fmol to 1.8 pmol. To determine K_M values for dCTP, its concentrations ranged from 1 to 1000 μM. K_M and k_{cat} were evaluated from the plot of the initial velocity versus the dCTP concentration using a hyperbolic curve-fitting program. Fold reduction of k_{cat} values is shown in parenthesis. Data from two to four independent experiments were plotted together and the correlation coefficients (R^2) were more than 0.97.

Protein	Template G			Template 8oxG			Template AP		
	k_{cat} (s^{-1})		K_M (μM)	k_{cat} (s^{-1})		K_M (μM)	k_{cat} (s^{-1})		K_M (μM)
REV1$^{(341-829)}$	0.073	(1.0)	0.33	0.032	(1.0)	9.1	0.13	(1.0)	11
F348A	0.065	(1.1)	0.79	0.027	(1.1)	3.1	0.053	(2.5)	32
S356A	0.068	(1.1)	10	0.033	(1.0)	7.7	0.014	(9.5)	78
R357A	0.025	(3.0)	79	0.017	(1.9)	57	0.0023	(57)	920
L358A	0.022	(3.4)	71	0.0042	(7.6)	29	0.0032	(42)	490
H359A	0.080	(1.0)	35	0.028	(1.1)	8.1	0.015	(9.2)	160

Table 3
Kinetic analysis of REV1$^{(341-829)}$ and mutants, R357A and L358A, for various DNA templates. Kinetic assays were performed for 5 min in 25 μl reaction mixtures using indicated templates with 88 fmol of REV1$^{(341-829)}$, 1.8 pmol of R357A and L358A. To determine K_M values for the templates, the concentrations ranged from 10 nM to 100 nM. The dCTP concentration was fixed at 100 μM. K_M and k_{cat} values were evaluated from the plot of the initial velocity versus the template concentrations using a hyperbolic curve-fitting program. Data from two to four independent experiments were plotted together and the correlation coefficients (R^2) were more than 0.94.

Protein	Template G K_M (nM)	Template 8oxG K_M (nM)	Template AP K_M (nM)
REV1$^{(341-829)}$	28	40	45
R357A	120	230	190
L358A	110	360	78

Table 4
Kinetic analysis of REV1$^{(341-829)}$ R357 mutants for dNMP incorporation with various DNA templates. Kinetic assays were performed for 5 min in 25 μl reaction solutions using 2.5 pmol of the indicated primer-templates. The enzyme concentrations ranged from 44 fmol to 88 fmol. To determine K_M values for dNTPs, the concentrations ranged from 1 to 1000 μM. K_M and k_{cat} were evaluated from the plot of the initial velocity versus the dCTP concentration using a hyperbolic curve-fitting program. Data from two to four independent experiments were plotted together and the correlation coefficients (R^2) were more than 0.95.

dNTP	Template G		Template 8oxG		Template AP	
	k_{cat} (s^{-1})	K_M (μM)	k_{cat} (s^{-1})	K_M (μM)	k_{cat} (s^{-1})	K_M (μM)
REV1$^{(341-829)}$						
G	0.097	300	0.014	72	0.0027	260
A	0.0037	420	0.00075	95	0.00035	680
T	0.048	200	0.014	79	0.0033	410
C	0.073	0.33	0.032	9.1	0.13	11
R357A						
G	0.097	23	0.043	27	0.014	190
A	0.080	48	0.028	56	0.0032	130
T	0.0058	100	0.0098	68	0.0020	580
C	0.025	79	0.017	57	0.0023	920
R357K						
G	0.014	340	0.0075	310	0.00042	380
A	0.027	210	0.012	88	0.0010	240
T	0.028	100	0.015	84	0.0015	270
C	0.042	31	0.045	82	0.0032	380
R357S						
G	0.088	25	0.037	9.2	0.014	170
A	0.047	130	0.023	44	0.0023	450
T	0.013	68	0.0078	35	0.0022	770
C	0.035	84	0.014	21	0.0025	960

Discussion

Although REV1 is a member of Y-family DNA polymerases and the amino acid sequence is well conserved among the members, its catalytic activity is restricted to utilization of dCTP as the dNTP source with a preference for a guanine residue as the template. Deletion analyses here revealed that an extra domain named the N-digit is essential for dCMP transferase activity of REV1, as reported previously [11,12]. This domain is conserved only in the REV1 family but not other Y-family polymerases, suggesting a crucial role for dCMP transferase activity. In this study, we determined for the first time the K_M values for templates. When each of R357 and L358 residues was replaced with alanine, the K_M values were increased. Interestingly, the defect of L358A was not as severe with template F as with the templates G and 8oxG, suggesting that the leucine residue might be crucial for binding to template G and damaged bases, but not the AP site. This is consistent with the model from the crystal structure and suggests that the leucine residue evicts template G from the DNA helix, then taking up much of the vacated space [12]. L358 could thus play a positive role in pushing out the base moiety. In this situation, R357 forms a hydrogen bond with the 5′ phosphate of the ejected template G [12]. Lack of this interaction on the R357A mutant could result in lowered affinity for template DNA.

When the R357 residue was replaced with others, the specificity for dCTP was altered. The kinetic analysis demonstrated that the arginine residue has a crucial function for selective utilization of dCTP. This result also is in good agreement with the model suggested by the crystal structure that the arginine residue forms hydrogen bonds with the cytidine residue of an incoming dCTP [12]. Besides, other amino acid residues surrounding the nucleotide binding pocket could also interact with the cytidine residue, since R357K mutant still retained a significant selectivity for dCTP. Furthermore, our analysis using mutants revealed that the nucleotide binding pocket has a significant but latent affinity for dGTP. When the R357 residue was replaced with other amino acids, in most of the cases, the enzyme lost affinity for dCTP, whereas an affinity for dGTP was obtained. Only in the case of the lysine was the affinity for dGTP rather reduced. It has been established that utilization of dGTP is an intrinsic property of wild-type REV1 [7–10,15]. The results suggest that surrounding amino acid residues in the nucleotide binding pocket except for the R357 residue probably have the potential to stabilize incoming dGTP. A positive charge of arginine or lysine could prevent such interaction with dGTP. Therefore, we suggest that R357 has two functions, which are specific interaction with dCTP and prevention of dGTP binding. We propose that both direct and indirect mechanisms ensure specificity for dCTP.

Our results also demonstrated significance of the SRLH motif for reaction with template AP sites. Mutations not only in R357 and L358 residues, but also S356 and H359, much reduced the transferase activity. Especially, the L358 residue could optimize the binding to a template AP site by occupying the empty space. A SRLH motif could be required for accurate arrangement of the template AP site and dCTP with the active site of REV1.

Many studies have demonstrated in yeast that the deoxycytidyl transferase activity of Rev1 is responsible for bypass synthesis of AP sites in different experimental systems, in which a gapped plasmid [16,17] or oligonucleotides containing an AP site [18–20] were transfected into yeast cells. Furthermore, expression of altered human uracil-DNA glycosylases that remove undamaged cytosines or thymines, was found to result in Rev1 dependent incorporation of dCMP opposite template AP site, generated by the glycosylases in yeast cells [21]. In spite of the elegant mechanisms of the enzyme to ensure incorporation of dCTP [11,12] and accumulating *in vivo* evidence, biological significance for insertion of dCMP is still obscure. In this study, we found novel mutants, which can incorporate dGMP with higher efficiency than dCMP. These could be useful for further analysis *in vivo* to address the biological significance for insertion of dCMP.

In conclusion, our experimental data suggest functional roles of conserved amino acid residues involved in substrate discrimination and template binding of the human REV1 protein. The proposed molecular mechanisms are supported by the model reported recently from crystallography. Furthermore, the mutants obtained in this study should facilitate further analysis *in vivo* to address the biological significance for insertion of dCMP by REV1.

Conflict of interest

None.

Acknowledgments

We are grateful to Kumiko Mizuno, Tomoka Nakashima, Masako Okii, Fumie Okubo, Kazumi Shimamoto, Hatsue Wakayama, and Mai Yoshida for their laboratory assistance. This work was supported by Grants-in-Aid from the Ministry of Education, Culture, Sports, Science and Technology of Japan (to Y.M. and K.K.), by the 21st Century Center of Excellence program from the Ministry of Education, Culture, Sports, Science and Technology of Japan (to K.K.), by Health and Labour Science Research Grants (to K.K.) and by Grants-in-Aid for Cancer Research from the Ministry of Health, Labour and Welfare (to K.K.). J.P. was supported by a JSPS Research Fellowship for Young Scientists.

References

[1] S.D. McCulloch, T.A. Kunkel, The fidelity of DNA synthesis by eukaryotic replicative and translesion synthesis polymerases, Cell Res. 18 (2008) 148–161.
[2] H. Ohmori, E.C. Friedberg, R.P. Fuchs, M.F. Goodman, F. Hanaoka, D. Hinkle, T.A. Kunkel, C.W. Lawrence, Z. Livneh, T. Nohmi, L. Prakash, S. Prakash, T. Todo, G.C.

Walker, Z. Wang, R. Woodgate, The Y-family of DNA polymerases, Mol. Cell 8 (2001) 7–8.
[3] C. Masutani, R. Kusumoto, S. Iwai, F. Hanaoka, Mechanisms of accurate translesion synthesis by human DNA polymerase η, EMBO J. 19 (2000) 3100–3109.
[4] S. Prakash, R.E. Johnson, L. Prakash, Eukaryotic translesion synthesis DNA polymerases: specificity of structure and function, Annu. Rev. Biochem. 74 (2005) 317–353.
[5] J.R. Nelson, C.W. Lawrence, D.C. Hinkle, Deoxycytidyl transferase activity of yeast REV1 protein, Nature 382 (1996) 729–731.
[6] C.W. Lawrence, Cellular roles of DNA polymerase ζ and Rev1 protein, DNA Repair 1 (2002) 425–435.
[7] Y. Zhang, X. Wu, O. Rechkoblit, N.E. Geacintov, J.S. Taylor, Z. Wang, Response of human REV1 to different DNA damage: preferential dCMP insertion opposite the lesion, Nucleic Acids Res. 30 (2002) 1630–1638.
[8] Y. Masuda, M. Takahashi, S. Fukuda, M. Sumii, K. Kamiya, Mechanisms of dCMP transferase reactions catalyzed by mouse Rev1 protein, J. Biol. Chem. 277 (2002) 3040–3046.
[9] Y. Masuda, K. Kamiya, Biochemical properties of the human REV1 protein, FEBS Lett. 520 (2002) 88–92.
[10] L. Haracska, S. Prakash, L. Prakash, Yeast Rev1 protein is a G template-specific DNA polymerase, J. Biol. Chem. 277 (2002) 15546–15551.
[11] D.T. Nair, R.E. Johnson, L. Prakash, S. Prakash, A.K. Aggarwal, Rev1 employs a novel mechanism of DNA synthesis using a protein template, Science 309 (2005) 2219–2222.
[12] M.K. Swan, R.E. Johnson, L. Prakash, S. Prakash, A.K. Aggarwal, Structure of the human Rev1–DNA–dNTP ternary complex, J. Mol. Biol. 390 (2009) 699–709.
[13] Y. Masuda, M. Takahashi, N. Tsunekuni, T. Minami, M. Sumii, K. Miyagawa, K. Kamiya, Deoxycytidyl transferase activity of the human REV1 protein is closely associated with the conserved polymerase domain, J. Biol. Chem. 276 (2001) 15051–15058.
[14] Y. Masuda, K. Kamiya, Role of single-stranded DNA in targeting REV1 to primer termini, J. Biol. Chem. 281 (2006) 24314–24321.
[15] C.A. Howell, S. Prakash, M.T. Washington, Pre-steady-state kinetic studies of protein-template-directed nucleotide incorporation by the yeast Rev1 protein, Biochemistry 46 (2007) 13451–13459.
[16] P.E. Gibbs, C.W. Lawrence, Novel mutagenic properties of abasic sites in *Saccharomyces cerevisiae*, J. Mol. Biol. 251 (1995) 229–236.
[17] J.R. Nelson, P.E. Gibbs, A.M. Nowicka, D.C. Hinkle, C.W. Lawrence, Evidence for a second function for *Saccharomyces cerevisiae* Rev1p, Mol. Microbiol. 37 (2000) 549–554.
[18] C. Otsuka, S. Sanadai, Y. Hata, H. Okuto, V.N. Noskov, D. Loakes, K. Negishi, Difference between deoxyribose- and tetrahydrofuran-type abasic sites in the *in vivo* mutagenic responses in yeast, Nucleic Acids Res. 30 (2002) 5129–5135.
[19] C. Otsuka, K. Kobayashi, N. Kawaguchi, N. Kunitomi, K. Moriyama, Y. Hata, S. Iwai, D. Loakes, V.N. Noskov, Y. Pavlov, K. Negishi, Use of yeast transformation by oligonucleotides to study DNA lesion bypass *in vivo*, Mutat. Res. 502 (2002) 53–60.
[20] C. Otsuka, N. Kunitomi, S. Iwai, D. Loakes, K. Negishi, Roles of the polymerase and BRCT domains of Rev1 protein in translesion DNA synthesis in yeast *in vivo*, Mutat. Res. 578 (2005) 79–87.
[21] P. Auerbach, R.A. Bennett, E.A. Bailey, H.E. Krokan, B. Demple, Mutagenic specificity of endogenously generated abasic sites in *Saccharomyces cerevisiae* chromosomal DNA, Proc. Natl. Acad. Sci. USA 102 (2005) 17711–17716.

doi:10.1016/j.jmb.2010.01.003 J. Mol. Biol. (2010) 396, 487–500

JMB

Available online at www.sciencedirect.com

ScienceDirect

ELSEVIER

DNA Replication-Coupled PCNA Mono-Ubiquitination and Polymerase Switching in a Human *In Vitro* System

Yuji Masuda*, Jinlian Piao† and Kenji Kamiya‡

Department of Experimental Oncology, Research Institute for Radiation Biology and Medicine, Hiroshima University, 1-2-3 Kasumi, Minami-ku, Hiroshima 734-8553, Japan

Received 14 August 2009; received in revised form 14 December 2009; accepted 5 January 2010
Available online
11 January 2010

Translesion DNA synthesis is a mechanism of DNA damage tolerance, and mono-ubiquitination of proliferating cell nuclear antigen (PCNA) is considered to play a key role in regulating the switch from replicative to translesion DNA polymerases (pols). In this study, we analyzed effects of a replicative pol δ on PCNA mono-ubiquitination with the ubiquitin-conjugating enzyme and ligase UBE2A/HHR6A/RAD6A–RAD18. The results revealed that PCNA interacting with pol δ is a better target for ubiquitination, and PCNA mono-ubiquitination could be coupled with DNA replication. Consequently, we could reconstitute replication-coupled switching between pol δ and a translesion pol, pol η, on an ultraviolet-light-irradiated template. With this system, we obtained direct evidence that polymerase switching reactions are stimulated by mono-ubiquitination of PCNA, depending on a function of the ubiquitin binding zinc finger domain of pol η. This study provides a framework for detailed analyses of molecular mechanisms of human pol switching and regulation of translesion DNA synthesis.

© 2010 Elsevier Ltd. All rights reserved.

Keywords: DNA polymerase switching; DNA replication; PCNA mono-ubiquitination; translesion DNA synthesis

Edited by J. Karn

Introduction

In living cells, DNA is exposed continuously to attack by endogenous reactive species, including oxygen radicals and metabolic intermediates, as well as environmental agents such as ionizing radiation, ultraviolet light (UV), and a variety of chemicals. Although resultant replication-blocking lesions are removed by nucleotide and base excision repair, significant numbers persist due to the balance between generation and excision. Therefore, cells need to be able to tolerate DNA damage during DNA replication.[1] The DNA damage tolerance pathway seems to act on single-stranded gaps[1,2] and therefore also is referred to as post-replication repair (PRR).[3] This process is separable into translesion DNA synthesis (TLS) and template switching (TS). In the TLS pathway, a number of nonessential DNA polymerases (pols) rescue stalled replication by extending the 3′-ends beyond the lesions. This process is essentially error-prone because of its utilization of a damaged template. With TS, the damage is bypassed by a copy choice mechanism using the newly synthesized sister chromatid as the template. For this reason, this process is deemed relatively error-free.[3]

In eukaryotes, a significant fraction of PRR is initiated by RAD6 (*Saccharomyces cerevisiae*)/UBE2A and UBE2B (in humans)- and RAD18-dependent ubiquitination at the lysine 164 residue of proliferating cell nuclear antigen (PCNA).[4–6] UBE2A and UBE2B, also known as HHR6A/RAD6A and HHR6B/RAD6B, respectively, are hereafter referred to as RAD6, applying the name of the yeast gene. RAD6, a ubiquitin-conjugating E2 enzyme, forms a tight complex with RAD18, a ubiquitin protein E3 ligase.[6–12] Mono-ubiquitination by the complex appears to be limited to PCNA already loaded onto DNA by replication factor C (RFC), demonstrated in *S. cerevisiae*[9,10] and humans.[13] It has been shown that Y-family translesion pols, which contain ubiquitin

*Corresponding author. E-mail address: masudayu@hiroshima-u.ac.jp.
† E-mail address: piao@hiroshima-u.ac.jp.
‡ E-mail address: kkamiya@hiroshima-u.ac.jp.

Abbreviations used: E1, ubiquitin-activating enzyme E1; PCNA, proliferating cell nuclear antigen; pol, DNA polymerase; PRR, post-replication repair; RFC, replication factor C; RF, replication factor; RPA, replication protein A; ssDNA, single-stranded DNA; TLS, translesion DNA synthesis; TS, template switching; UE, ubiquitin enzyme; UBZ, ubiquitin binding zinc finger; BSA, bovine serum albumin; EDTA, ethylenediaminetetraacetic acid.

0022-2836/$ - see front matter © 2010 Elsevier Ltd. All rights reserved.

binding motifs or ubiquitin binding zinc fingers (UBZs), are recruited by interaction with mono-ubiquitinated PCNA to allow TLS through damage sites.[14–18] Mono-ubiquitination can also be followed by poly-ubiquitination by the UBC13–MMS2 complex, an E2 ubiquitin-conjugating enzyme, and RAD5 (in *S. cerevisiae*)/SHPRH and HLTF (in humans) E3 ubiquitin ligases, leading to TS.[3,13,19–21]

Mono-ubiquitination of PCNA is considered to play a key role in regulation of PRR. In yeast, most TLS depends on PCNA mono-ubiquitination. However, in chicken DT40 cells, mono-ubiquitination of PCNA seems crucial, but not essential, for translesion synthesis.[22,23] The majority of the remaining TLS in the PCNA$^{(K164R)}$ background depends on REV1. The presence of distinct pathways in higher eukaryotes is very clear in PCNA$^{(K164R)}$ knock-in mice, in which only reduction of mutations at template A/T and a compensatory increase at G/C in immunoglobulin genes have been observed.[24] This phenotype is similar to that with pol η-deficient cells,[25–27] suggesting that PCNA mono-ubiquitination is closely linked to functions of pol η.

Mono-ubiquitinated PCNA accumulates on treatment of cells with DNA-damaging agents.[4,6,14,17,28,29] Recent reports have provided evidence that a significant proportion of PCNA mono-ubiquitination is constitutive, since accumulation is observed on inactivation of a de-ubiquitinating enzyme, USP1.[29–31] Importantly, in chicken DT40 cells, elevated levels of mono-ubiquitinated PCNA, which result from disruption of the *USP1* gene, do not increase mutagenesis at endogenously created DNA damage in the immunoglobulin locus.[31] This indicates that ubiquitination of PCNA is not sufficient for activating mutagenic translesion synthesis. In yeasts, it has been shown that PCNA is constitutively ubiquitinated during normal S phase.[28,32] For these reasons, the role of the RAD6–RAD18 complex in mono-ubiquitination of PCNA, its dependence on template damage, and its role in switching polymerases at stalled replication forks are not clear.

To address the molecular mechanisms underlying polymerase switching and its dependence on PCNA mono-ubiquitination by RAD6–RAD18 in mammals, we have established an *in vitro* reconstituted system. This system uses purified recombinant proteins, including pol δ, RFC, PCNA, replication protein A (RPA), ubiquitin-activating enzyme E1 (E1), the RAD6A–RAD18 complex, ubiquitin, and pol η. In this report, we described protein actions with this *in vitro* system.

Results

Reconstitution of PCNA mono-ubiquitination with recombinant human proteins *in vitro*

It has been suggested that mono-ubiquitinated PCNA mediates polymerase switching from replicative to translesion pols.[2] To address molecular mechanisms underlying mono-ubiquitination of PCNA and polymerase switching *in vitro*, we first established methods to obtain highly purified recombinant human replication factors (RFs, including RFC, PCNA, and RPA), ubiquitin enzymes (UEs, including E1, RAD6A–RAD18 complex, and ubiquitin), pol δ, and pol η (Fig. 1a)[33] from overproducing *Escherichia coli* cells by conventional column chromatography. The elution profile for each protein gave a sharp and symmetric peak from the gel-filtration column, demonstrating a quality sufficient for enzyme assays (data not shown).

Reactions for PCNA mono-ubiquitination *in vitro* have been established in *S. cerevisiae* and human systems.[9,10,13] Here, the reactions were reproduced using RPA-coated, singly primed mp18 single-stranded DNA (ssDNA) (Fig. 1b). The reaction condition was originally optimized for DNA replication,[33] and UEs were introduced to give saturated amounts with respect to mono-ubiquitination of PCNA. After

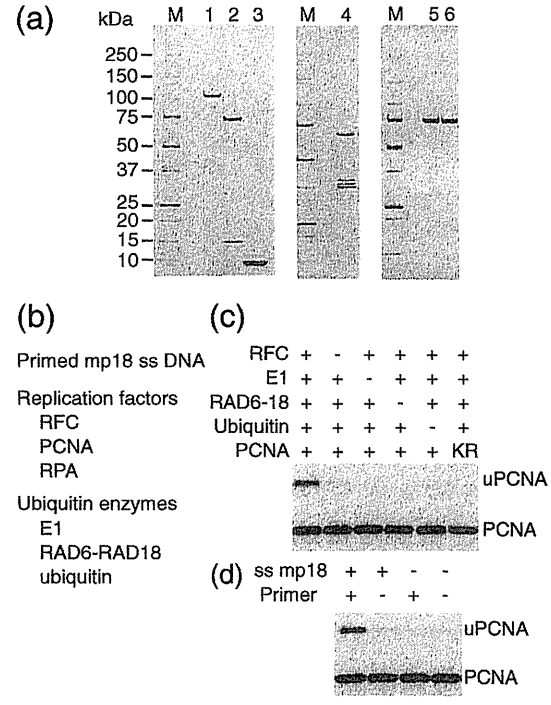

Fig. 1. Reconstitution of PCNA mono-ubiquitination. (a) Purified proteins in this study. Purified recombinant proteins, 500 ng (4.2 pmol) of E1 (lane 1), 650 ng (8.8 pmol) of RAD6A–RAD18 (lane 2), 500 ng (58 pmol) of ubiquitin (lane 3), 800 ng (3.6 pmol) of RFC$^{(P140N555)}$ (lane 4), 500 ng (6.4 pmol) of pol η (wild type) (lane 5), and 500 ng of pol η$^{(D652A)}$ (lane 6) were loaded on an SDS 5–20% gradient polyacrylamide gel and stained with Coomassie Brilliant Blue R-250. (b) Summary of the assay system for PCNA mono-ubiquitination. (c) Requirement of protein components for PCNA mono-ubiquitination. KR represents a mutant of PCNA, PCNA$^{(K164R)}$, in place of the wild type. (d) Requirement of DNA components for PCNA mono-ubiquitination. The reactions were carried out for 30 min. The indicated components were omitted from the reactions, and reaction products were analyzed by Western blotting using anti-PCNA antibodies. uPCNA represents mono-ubiquitinated PCNA.

incubation for 30 min at 30 °C, PCNA molecules were visualized by Western blotting. This assay detected a slower migrating band, the size corresponding to the mono-ubiquitinated PCNA (Fig. 1c and d), which reacted with anti-ubiquitin antibody (data not shown), indicating it to be mono-ubiquitinated PCNA. The PCNA ubiquitination depended on the protein components, RFC and UEs (Fig. 1c), and singly primed mp18 ssDNA (Fig. 1d). Inefficient ubiquitination was detected without RFC (Fig. 1c) or the primer (Fig. 1d), probably due to nonspecific interactions of the proteins with mp18 DNA forming a secondary structure. When PCNA was replaced with a mutant, $PCNA^{(K164R)}$, no products were detected (Fig. 1c). Biochemical activity of the mutant was essentially identical with that of wild type with respect to DNA replication with pol δ (Supplementary Fig. S1), indicating that the mutation did not affect the integrity of the molecule. These results suggested ubiquitin to be specifically conjugated to the lysine 164 residue in these reactions, as detected earlier *in vivo*[4] and *in vitro*.[9,21]

Mono-ubiquitination of PCNA interacting with pol δ

Since pol δ forms a complex with PCNA at the 3′-end during elongation reaction, we asked the question of whether such PCNA could act as a target for ubiquitination. To address this question, we used poly(dA)–oligo(dT) as a DNA source. It is well established that poly(dA)–oligo(dT) is an excellent substrate for pol δ in PCNA-dependent and RFC-independent reactions,[34–42] since PCNA molecules spontaneously are loaded onto DNA from the ends without RFC[43] as illustrated in Fig. 2a. Indeed, we confirmed powerful stimulation of DNA synthesis of pol δ by only the addition of PCNA without RFC and RPA under our assay conditions (Supplementary Fig. S2), suggesting functional interactions between PCNA and pol δ on the poly(dA)–oligo(dT) without RFC. Then, we analyzed PCNA mono-ubiquitination in the presence of UEs. As shown in Fig. 2a, we surprisingly found that mono-ubiquitination of PCNA was strongly stimulated by only the addition of pol δ as well as RFC, but not pol β (Fig. 2b). Importantly, the required amount of pol δ for ubiquitination was stoichiometric, rather than catalytic, to that for PCNA (1 pmol as trimers was present in the reaction mixture) (Fig. 2b), suggesting the possibility that PCNA interacting with either RFC or pol δ is able to be a target for ubiquitination.

To obtain additional evidence, we used 5′-biotinylated oligo(dT) for the assay. First, loading of PCNA was monitored by stimulation of DNA synthesis (Fig. 2c). Neither the biotin moiety at the 5′-end nor streptavidin itself affects polymerase reactions (Fig. 2c, lanes 2 and 3, data not shown). When streptavidin was preincubated with template DNA, the stimulatory effect of PCNA was canceled (Fig. 2c, lanes 4 and 5), and it was partially restored by addition of RFC (Fig. 2c, lanes 5 and 6). Importantly, the results were identical with those when PCNA was preincubated with the template DNA before addition of streptavidin (Fig. 2c, lanes 7–12), indicating the amount of PCNA molecules on DNA without pol δ to be negligible. These results suggested that spontaneously loaded PCNA is basically unstable but can remain on the DNA by interaction with pol δ. Next, mono-ubiquitination of PCNA was analyzed by addition of UEs (Fig. 2d). The results showed that stimulation of PCNA mono-ubiquitination by pol δ was markedly reduced by addition of streptavidin (Fig. 2d, lanes 3 and 4) and was partially restored by addition of RFC (Fig. 2d, lanes 4 and 5). Identical results were obtained when PCNA was preincubated with the template DNA before addition of streptavidin (Fig. 2d, lanes 6–10). These results supported the possibility that PCNA molecules, interacting with pol δ, are able to be ubiquitinated.

To determine whether the interaction between pol δ and PCNA affected efficiency of mono-ubiquitination, we performed the following experiments with isolated encircled PCNA molecules on plasmid DNA as the substrate (Fig. 2e). After loading reactions, DNA–PCNA complexes were separated from DNA-free PCNA by gel filtration and then fractions containing DNA–PCNA complexes were subjected to ubiquitination assays using nicked circular plasmids, since they well support PCNA mono-ubiquitination[13] (data not shown). For PCNA loading, a mutant RFC, $RFC^{(p140N555)}$, which was formed with a truncated RFC1 subunit that lacked a nonspecific DNA binding domain,[44] was employed. The benefit of using $RFC^{(p140N555)}$ for loading reactions is prevention of contamination due to nonspecific interactions between the DNA binding domain of RFC and DNA on subsequent gel filtration.[45] When purified fractions were reacted with UEs, we detected a small amount of ubiquitinated PCNA (Fig. 2f, lanes 2 and 9), suggesting that encircled PCNA is capable of ubiquitination without pol δ or RFC. To see the effects of RFC or pol δ, we then introduced these proteins into the reactions. Here, we detected increased products depending on the amounts of RFC (Fig. 2f, lanes 2–7) and pol δ (Fig. 2f, lanes 9–14), suggesting that both have the ability to stimulate the reaction. In this experiment, it was critical to confirm that the PCNA–DNA complex is stable under our assay conditions, as an important control. If a significant fraction of PCNA dissociated spontaneously during incubation, the stimulation might be a consequence of stabilization of PCNA by interaction with pol δ. To assess the stability of encircled PCNA, we divided the purified complexes into three. One sample was immediately reacted with UEs for 30 min; others were preincubated for 30 min without RAD6A–RAD18 and E1 in the presence or absence of a restriction enzyme, HincII, for linearization of the plasmid, and then the reaction was carried out for a further 30 min by introduction of RAD6A–RAD18 and E1 (Supplementary Fig. S3a). The results of Western blotting showed that the capacities for ubiquitination were not changed before and after the incubation for 30 min but halted by linearization of DNA

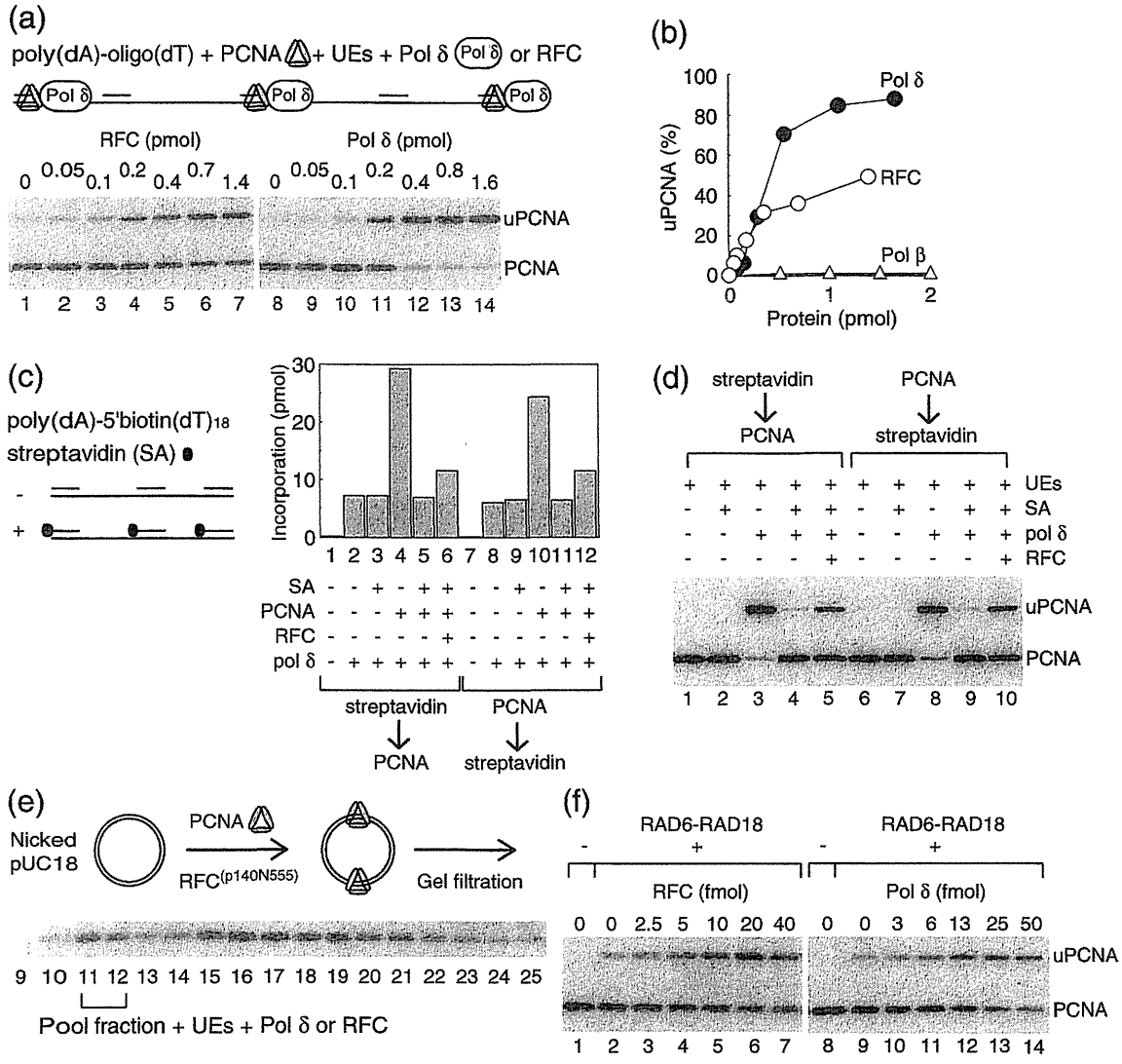

Fig. 2. Mono-ubiquitination of PCNA interacting with pol δ. (a) Titration of pol δ and RFC in the PCNA mono-ubiquitination reaction with poly(dA)–oligo(dT) as the DNA source. The experimental design is shown in the upper part. In this reaction, poly(dA)–oligo(dT) and PCNA were incubated with UEs. Amounts of oligo(dT) as primer termini were 0.9 pmol in the reaction. Indicated amounts of RFC or pol δ were introduced into the reaction mixtures followed by incubation for 30 min. Reaction products were analyzed by Western blotting using anti-PCNA antibodies. (b) Quantification of mono-ubiquitinated PCNA shown in (a), and with pol β. Titration of pol β was performed as for pol δ described in (a). The signal intensity detected by a CCD camera was quantified and plotted as the relative amount of the mono-ubiquitinated form. (c) DNA synthesis on poly(dA)–5′ biotinylated oligo(dT). The 5′ biotinylated oligo(dT), 18-mer, was annealed with poly(dA). In lanes 1 to 6, DNA was incubated with streptavidin (SA) on ice for 10 h and then mixed with PCNA. In lanes 7 to 12, DNA was incubated with PCNA on ice for 1 h and then incubated with streptavidin on ice for 10 h. Replication reactions were carried out for 10 min under standard reaction conditions with pol δ (220 fmol) and RFC (1.4 pmol) as indicated. (d) PCNA mono-ubiquitination assays with poly(dA)–5′ biotinylated oligo(dT). The substrate DNA was prepared as described in (c). Reactions were carried out for 10 min under standard reaction conditions with pol δ (840 fmol) and RFC (1.4 pmol) as indicated. Reaction products were analyzed by Western blotting using anti-PCNA antibodies. (e) Purification of PCNA assembled on nicked circular DNA by gel-filtration chromatography. A schematic representation of the experimental design is shown in the upper part. After loading PCNA on nicked circular DNA by RFC$^{(p140N555)}$, the products were passed through a gel-filtration column. Indicated fractions were analyzed by Western blotting. Encircled PCNA on DNA eluting in the void volume of the gel filtration in fractions 11 and 12 was subjected to ubiquitination reactions (f). (f) PCNA mono-ubiquitination assays with purified PCNA–DNA complexes. Encircled PCNA (e) was incubated with the indicated amounts of RFC or pol δ in the presence of UEs. Reaction products were analyzed by Western blotting using anti-PCNA antibodies. uPCNA represents mono-ubiquitinated PCNA.

(Supplementary Fig. S3b), indicating that encircled PCNA is the target for ubiquitination and spontaneous dissociation of PCNA was negligible under the reaction conditions. The result could also rule out the possibility of contamination of RFC$^{(p140N555)}$. Because RFC$^{(p140N555)}$ has the potential to unload encircled PCNA,[46] if it were present in the reactions, the result would be reduction of the capacity for